MODELING AND COMPENSATION FOR BIODYNAMIC FEEDTHROUGH IN BACKHOE OPERATION

A Thesis
Presented to
The Academic Faculty

by

Heather C. Humphreys

In Partial Fulfillment
of the Requirements for the Degree
Master of Science in Mechanical Engineering in the
Mechanical Engineering Department

Georgia Institute of Technology
December 2010

MODELING AND COMPENSATION FOR BIODYNAMIC FEEDTHROUGH IN BACKHOE OPERATION

Approved by:

Professor Wayne J. Book, Advisor
Mechanical Engineering Department
Georgia Institute of Technology

Professor William Singhose
Mechanical Engineering Department
Georgia Institute of Technology

Professor Steven X. Jiang
Department of Industrial and Systems Engineering
North Carolina Agricultural and Technological State University

Date Approved: November 15, 2010

To my grandfather,

William Edgar Humphreys, Jr.

ACKNOWLEDGEMENTS

I am grateful to many people for helping me work through this master's project. First, I want to thank my advisor Dr. Wayne Book for his wisdom, guidance and support. He seems to always manage the balance between giving me the necessary guidance to avoid heading down a dead-end path while allowing me to make my own mistakes and learn from them. I also want to thank my other committee members, Dr. Bill Singhose and Dr. Steven Jiang, for their thorough review of my work and many suggestions.

I also want to thank our research engineer J.D. Huggins. He has been an excellent technical resource. He has always made himself available, at most any time of day, at all the times when there were technical problems to work through just before deadlines. I also want to thank previous researchers Dr. Matt Kontz and Joe Frankel for developing a reliable and well-documented testbed.

I am also grateful to our corporate sponsors and the NSF Center for Compact and Efficient Fluid Power. In particular, I want to express thanks to John Deere, Caterpillar and LifeModeler. I also want to express my appreciation for support from the National Science Foundation and the Air Force Office of Scientific Research.

I also want to thank all of the members of the Intelligent Machine Dynamics Laboratory. I am honored to be a part of their group. My colleagues are always available to help me work through any technical challenge.

Finally, I want to thank my friends and family, in particular my parents, for their support. They have been understanding of the many times when I became consumed by my work, and they have provided much needed encouragement in the frustrating times.

TABLE OF CONTENTS

LIST OF TABLES

LIST OF FIGURES

SUMMARY

Biodynamic feedthrough occurs in many types of operator controlled machines where the operator is a passenger and the motion of the controlled machine excites motion of the human operator, creating unwanted feedback. It is a significant cause for control performance degradation in backhoes. In this research, the problem of biodynamic feedthrough is investigated in a backhoe control system. For simplification, the system is limited to a single degree of freedom. Several controller based approaches are investigated to reduce cab vibration, while maintaining cylinder tracking performance. These controllers are tested in hardware, with and without the human operator and associated biodynamic feedthrough. The effect of this cab vibration reduction on biodynamic feedthrough is tested in a small set of human subject tests. The results indicate that some vibration reduction and improvement in the operator's control performance can be achieved by adding cab vibration compensation.

This research is presented in seven chapters. Chapter 1 gives an introduction to the problem of biodynamic feedthrough and the approach used in this work. Chapter 2 provides background on mobile hydraulic machine control, biodynamic feedthrough, and control of flexible systems. In Chapter 3, models of each of the major dynamic components are developed. These models are used in Chapter 4 for the development of several different types of controllers, with the purpose of achieving acceptable cylinder tracking performance while minimizing cab motion excitation. The stability of the system with biodynamic feedthrough is analyzed. Chapter 5 presents simulation and hardware testing results in terms of cylinder position tracking and cab vibration, omitting the human operator and biodynamic feedthrough. Chapter 6 presents results

for human subject tests, with each controller type, with the operator both on and off the tractor. Finally, conclusions from these tests and potential areas for future work are described in Chapter 7.

CHAPTER I

INTRODUCTION

1.1 Problem Description

This research is part of a larger group effort to improve user interfaces and operability of mobile hydraulic machines, particularly backhoes and excavators. One widely recognized problem in operation of such machines is biodynamic feedthrough. This phenomenon occurs when motion of the controlled machine excites motion of the human operator, which is fed back into the control device. This unwanted input can cause limit cycles or even instability. In operation of backhoes and excavators, biodynamic feedthrough causes significant control performance degradation.

Biodynamic feedthrough can occur in operation of many types of vehicles and machines with the operator as a rider. This phenomenon has been widely studied in the case of fighter pilots. The unwanted input resulting from biodynamic feedthrough can be affected by many different factors, including the mapping and scaling between operator inputs and machine outputs, the dynamics of the machine, the input device and the human body. For instance, imagine steering a car through a tight turn using a joystick instead of a steering wheel. The acceleration of your body would be translated into the joystick, causing unwanted input. But with a steering wheel, operator input about the roll axis is mapped to vehicle motion about the yaw axis. In the case of the accelerator pedal, the operator's heel is fixed to the car. The driver is controlling only two degrees of freedom, fore-aft linear motion and yaw rotation. In such cases, biodynamic feedthrough can be mitigated by decoupling the axes of the input and output or by stabilizing the operator's wrist or ankle. However, in cases where the operator controls more degrees of freedom and experiences larger

accelerations, such as fighter jets or excavators/backhoes, these methods are often not sufficient to mitigate biodynamic feedthrough problem. In addition, the unwanted input resulting from biodynamic feedthrough cannot be measured during operation, since it cannot be decoupled from the operator's desired command. This unwanted addition to the operator's command is highly correlated with the output and acts as a feedback loop.

1.2 Main Goals

The main goals of this research are (1) to investigate and model the effect of biodynamic feedthrough on a backhoe control system, and (2) to develop compensation to reduce the adverse effects of biodynamic feedthrough. The system contains four main dynamic components which contribute to the biodynamic feedthrough effect: the valve and cylinder dynamics, the structural dynamics of the tractor/backhoe system, the dynamics of the input device itself, and the human body biomechanics. In more quantitative terms, these goals translate into a reduction of the resonant peak in cylinder output resulting from the biodynamic feedthrough and improved operator tracking performance.

In order for a compensation method to be applicable in industry, several other requirements come into play. First, the compensation must be robust to variations in many parameters. Some examples of causes of parameter variations include: (1) changes in the human operator, (2) varying loading conditions, (3) variation in the tractor-to-ground stiffness resulting from variations in soil, tires, and use of outriggers, (4) changes in the dynamics of the valve/cylinder and tractor/backhoe structure resulting from the changing backhoe arm configuration, and (5) changes in machine response resulting from machine component wear. The selected compensation method should also be reliable; addition of sensors and other components should be minimized to reduce the risk of component failures, and the control algorithms should be robust

to such failures. Additionally, added cost for compensation should be minimized.

1.3 Related Research

This research is part of a larger collaborative effort to improve user interfaces for mobile hydraulic machines, particularly backhoes and excavators, which involves investigations into several different improvements. Some of these will be described in more detail in a later section. One particularly relevant area of research is the mapping between the input device and the machine output. Conventional backhoe controls use two joysticks for rate control of each individual joint as shown in Fig. 1.

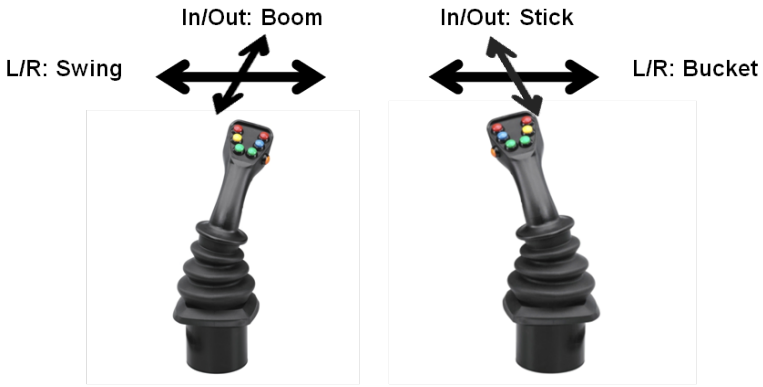

Figure 1: Conventional 2-joystick mappings

Several studies have investigated different mappings from input devices to backhoe/excavator arm motion. One proposed alternative to the conventional two-joystick approach is the use of a multiple degree-of-freedom input device for coordinated position control. With this method, as the operator's hand moves up, the bucket moves up; as the operator's hand moves forward, the bucket moves forward, and so on. This method has shown to be much more intuitive for inexperienced operators. A new backhoe testbed called the Haptically Enhanced Robotic Excavator (HEnRE) was developed in Georgia Tech's Intelligent Machine Dynamics Laboratory (IMDL) by Dr. Matt Kontz and several other researchers ([20], [8]). This testbed is used in this research and shown in Fig. 2, and it is described in detail in a later section.

Figure 2: Haptically Enhanced Robotic Excavator (HEnRE) Testbed

The HEnRE system uses the SensAble OmniTM six degree-of-freedom input device for coordinated position control.

Figure 3: SensAble OmniTM

One disadvantage of the coordinated position control is that it is more susceptible to biodynamic feedthrough than conventional rate control, since it does not have the smoothing effect of the integration between the operator's input and the backhoe position output. Biodynamic feedthrough presents a major obstacle preventing this new interface from moving forward with industry; therefore, this research study focuses on the coordinated position control using the SensAble Omni.

1.4 Approach

Initially, several different approaches to biodynamic feedthrough compensation were considered; those can be divided into four main concepts. Figure 4 represents the biodynamic feedthrough loop in backhoe valve/cylinder control. In general, the goal is to minimize the effects of signal $H(s)$ in Fig. 4 on the system output.

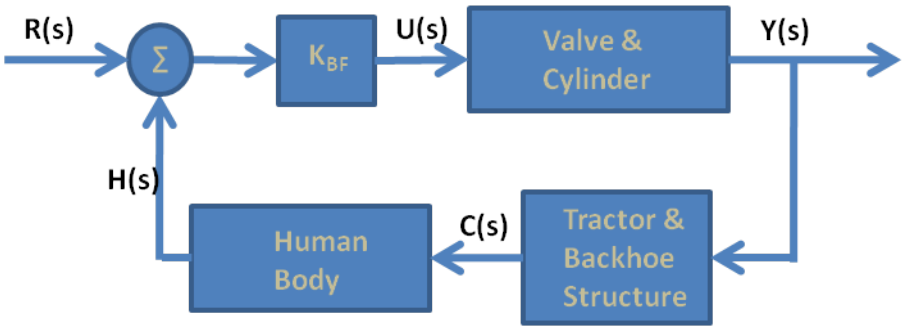

Figure 4: Basic biodynamic feedthrough block diagram

The signal $R(s)$ represents the operator's intended command input, $U(s)$ represents the valve command, $Y(s)$ represents the cylinder position output, $C(s)$ represents cab motion, and $H(s)$ represents the unwanted motion of the operator's hand resulting from the biodynamic feedthrough. The undesirable hand motion $H(s)$ cannot be directly measured in operation, since it cannot be decoupled from the intended hand motion $R(s)$. One possibility is to estimate the undesirable input resulting from the biodynamic feedthrough and subtract that estimate from the valve command signal. This estimate of signal $H(s)$ can be obtained from a measurement of signal $C(s)$ and a model of the human body dynamics. Some researchers have tried this approach on single degree-of-freedom (DOF) vehicles. This approach requires an accurate model of the human body dynamics. This approach was used in [32], in which the designers used a customized biomechanics model obtained by system identification for each human test subject. The human operator biomechanics are known to vary significantly, and such a customized controller design for each operator is impractical for backhoe operation. Other studies have addressed variation in the human operator

by robust control strategies, but none have clearly defined ranges or expected values for human body parameter variation values.

Another basic concept to overcome the adverse effects of biodynamic feedthrough is to scale the required operator input such that the required force and/or displacement generated by the hand (signal $R(s)$) are much larger than the unwanted force and displacement resulting from the feedthrough effect (signal $H(s)$). This scaling can be achieved through modifications to the input device, by increasing its workspace, increasing the damping force, or increasing the spring return force in rate control mode. These approaches are all detrimental to the ergonomics of the user interface, causing increased operator fatigue.

A third approach involves reducing the cab vibration so that the human is not excited. Reduction of cab motion could be achieved by several different methods, including filtering of the valve command signal, input shaping the command signal, active vibration control using additional actuators mounted on the cab, or active vibration control using the backhoe arm itself. Active vibration control using additional actuators was deemed too cost prohibitive. However, both the filtering approach and the active vibration control method using the backhoe arm itself are viable options. Both of these methods are investigated in this research. For the filtering approach, a notch filter can be placed at each structural natural frequency, minimizing the excitation of those frequencies by the backhoe arm. The gain K_{BF} corresponds to the scaling between the Omni and backhoe, and it is sufficiently small that the closed loop pole locations are relatively close to the open loop pole locations; therefore, the feedback does not significantly diminish the effects of a filter. This method has the advantage of simplicity, but it does not compensate for disturbances or nonlinear effects. Active vibration control using the working arm for vibration damping uses the cab acceleration measurement as feedback; therefore, it may compensate for some disturbances and nonlinear effects. However, it is a much more complex controller

design and requires more extensive modeling; in addition, the backhoe arm has competing objectives of tracking the operator's command input and actively reducing cab acceleration.

1.5 Major Assumptions and Simplifications

Biodynamic feedthrough presents a very complex problem in the control of high degree-of-freedom machines such as backhoes and excavators. As an initial step, in order to make the problem more manageable, some significant simplifications and assumptions were made.

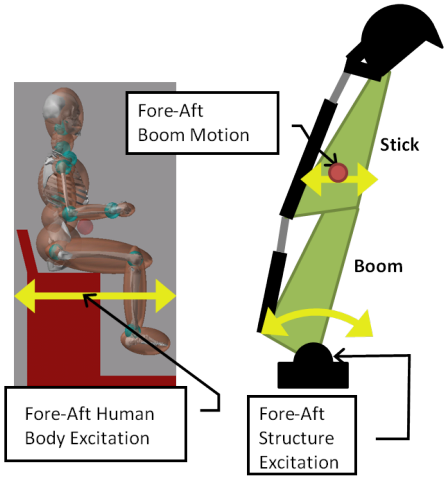

Figure 5: Single degree-of-freedom approximation

(1) The system is limited to a single degree-of-freedom, fore-aft motion with small motions of the arm. This approximation is made possible by operating the backhoe only within a small angle approximation and in a configuration that produces primarily fore-aft motion of the backhoe arm, the cab, and the human body. This approximation is illustrated in Fig. 5.

In addition, only one joint is actuated at a time, either the stick or the boom. The arm is limited to small motions in each case, which produce primarily fore-aft motion of the cab and human.

(2) The operator's response to the cab vibration is assumed to be completely

involuntary; any cognitive effects on the system dynamics are neglected. During operation of the backhoe, the human operator adds a visual/cognitive/neuromuscular feedback that does affect the dynamics of the system; in fact, the operator typically adjusts his own feedback dynamics to some extent in order to optimize the machine control [27]. In this study, any cognitive dynamic effects are neglected; the operator is assumed to have no real-time sensory feedback on the backhoe position. Previous researchers have noted that biodynamic feedthrough occurs at frequencies much higher than any human cognitive bandwidth; therefore, the effect of biodynamic feedthrough is primarily of involuntary nature [1].

(3) Nonlinearities are neglected in the control design. This system is known to include many forms of nonlinearities resulting from the hydraulic system, the kinematics of the arm and human body, the complex and nonideal structure of the tractor, etc. There are a large number of nonlinear effects which would be difficult to decouple and identify. Some of these effects are investigated and tested in simulations, but in general, linear models for all dynamic components are used for controller design.

The thesis is organized as follows. Chapter 2 provides background on the backhoe hardware system, biodynamic feedthrough, and several forms of vibration control in different types of machinery. In Chapter 3, models of each of the major dynamic components of the system are developed. In Chapter 4, several different types of controller designs are developed for the system, and their stability is analyzed with biodynamic feedthrough. Chapter 5 describes both hardware and simulation experiments to evaluate the various controllers' abilities to reduce cab vibration while providing acceptable tracking performance. Chapter 6 describes a set of human subject experiments to evaluate the biodynamic feedthrough compensation.

CHAPTER II

BACKGROUND

2.1 Backhoe User Interface Design and HEnRE

While the industry standard in backhoe control has remained as the same 2-joystick, 4-DOF mapping for several decades, several researchers have investigated the use of coordinated control. One well-known example is that of Lawrence [21], who implemented coordinated velocity control with and without force feedback, using a 5-DOF input device. Another advanced user interface for a backhoe has been developed in the Intelligent Machine Dynamics Laboratory (IMDL) at Georgia Tech, called the Haptically Enhanced Robotic Excavator (HEnRE), which uses coordinated position control with haptic feedback. The HEnRE system is described in [8], [20], [16], [17] and [18], and it is pictured in Fig. 6.

Figure 6: Haptically Enhanced Robotic Excavator (HEnRE) Testbed with SensAble Omni

The HEnRE system uses a SensAble Omni commercial six degree-of-freedom (DOF) haptic display input device, shown in Fig. 3. The Omni is mounted beside the tractor seat, in a manner similar to conventional electronic joysticks. It enables coordinated position-to-position mapping from the input device to the backhoe arm, allowing the use of a computer for the inverse kinematics calculations. In contrast, conventional backhoe user interfaces use position-to-velocity mapping with two separate 2-DOF joysticks (totaling 4-DOF) to provide four independent inputs to control four actuators on the backhoe arm. Tests indicate that the coordinated control interface used on HEnRE provides much more intuitive operation [20].

While many systems using coordinated position control of backhoes and excavators have been developed, one unique feature of the HEnRE system is its use of more industry-standard, low cost components. It has the economic advantage that it utilizes proportional valves and a constant displacement pump, rather than servo valves and variable displacement pumps, which tend to be cost-prohibitive; methods for efficient control of the pump for this system are discussed in [17]. Methods for providing haptic feedback to represent load forces and system limitations are discussed in [16] and [18]. The system uses a 4410 series John Deere tractor with a Model 47 backhoe. It has been retrofitted with Sauer-Danfoss PVG-32/PVES electro-hydraulic (EH) closed-center proportional directional valves and an electro-proportional relief valve. It uses the original constant displacement pump. The system includes a wide array of sensors, including Balluff magnetorestrictive position sensors for each cylinder. An Analog Devices 3-axis MEMS accelerometer is mounted on the base of the tractor seat.

The backhoe controller uses software written using MATLAB/Simulink with xPC Target for real-time control implemented on a dedicated PC-104 target. A separate Windows host PC is used for real-time control development, and that same PC is used for control of the SensAble Omni using C/C++ with the SensAbleTM libraries.

The real-time target PC-104 and the Windows PC controlling the SensAble Omni communicate via Ethernet with UDP protocol, and the target sample rate is set to 1000 Hz.

Some modifications were made to the off-the-shelf SensAble Omni input device. The original device has three degrees-of-freedom that are actuated, the base rotation, upper arm and lower arm links. The three degrees-of-freedom of the wrist are not actuated. With the original end effector link, any force created by the Omni creates a moment about the operator's grip, as shown in Fig. 7.

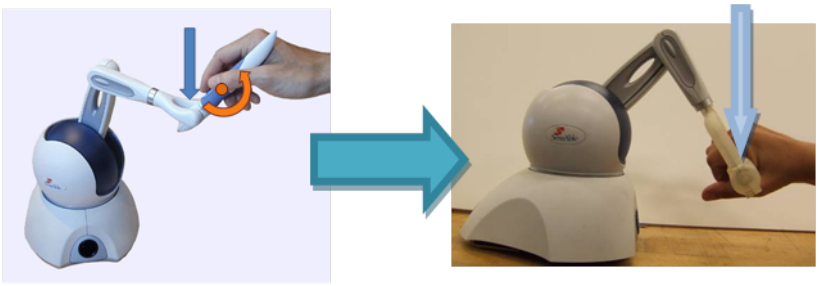

Figure 7: Changes to SensAble Omni

The modifications to the grip end effector move the operator's grip to be aligned with the lower arm link, eliminating the unwanted moment. The wrist yaw degree-of-freedom is fixed in place, reducing the input device to 5-DOF. This more closely matches with the backhoe's 4-DOF configuration. The backhoe also does not have a wrist roll degree-of-freedom, but this joint is used passively in the input device for ergonomic purposes. In the previously developed full 4-DOF control system, the wrist pitch angle controls the backhoe bucket. In this testing, only the fore-aft component of the input device motion is used.

2.2 Biodynamic Feedthrough

Biodynamic feedthrough is a widely recognized problem in the area of high-performance aircraft, and it has been an area of research in the aerospace industry for several decades. It is also significant in control of mobile hydraulic equipment, though

it has received less attention in this area. Backhoe user interface designers claim that the new electronic joysticks have more problems with biodynamic feedthrough than the earlier manual joysticks. Both versions of joysticks are used as rate-controllers. The earlier manual joysticks tend to have larger workspace sizes and more damping; these characteristics make the earlier manual joysticks less susceptible to biodynamic feedthrough but more fatiguing for an operator. The HEnRE system uses position control.

Only a few publications on biodynamic feedthrough consider hydraulic equipment applications. In [3], a similar investigation on biodynamic feedthrough in excavator operation is performed using simplified mass-spring-damper models, though the experimental validation of the modeling is limited. Another simulation-only investigation for a similar problem is presented in [24]. This study provides a very detailed planar model of the hydraulic and mechanical dynamics of an excavator with a manual control joystick. This particular excavator has suspension between the cab and chassis; the joystick is mounted to the cab and connected to a valve mounted in the chassis. In this case, the relative motion between the cab and chassis creates a control input to the valve, such that unstable behavior occurs when this signal is outside the deadband of the valve. The operator also contributes to this instability, but authors note that in some cases oscillations continue even after the operator releases the joystick. The paper focuses on the modeling of the system and understanding the instability, rather than solving the instability problem.

An in-depth study on biodynamic feedthrough was performed by Systems Technology, Inc., under a contract for the US Air Force [14], [1]. It focuses on development of lumped-parameter biomechanical models for the human pilot, for the purpose of developing software to simulate the interaction between human body dynamics and structural modes in manual control systems. Human experiments were performed to measure the involuntary biodynamic response to seat excitation, but the experiments

assumed a semisupine, or leaned back, pilot body position which make the models not directly applicable to the backhoe. The publications present detailed human body models for vertical and lateral motion, but they do not present detailed fore-aft models. In general, results indicate that biodynamic feedthrough effects are primarily of involuntary nature; any cognitive or neuro-muscular compensation is negligible. They also note that it is the difference between the human body motion and cockpit motion that results in unwanted input; measures taken to isolate the pilot or input device from cockpit vibration would likely aggravate the biodynamic feedthrough effects. Another study, discussed in [34], presents a model of the human pilot's arm for lateral motion only. Two other investigations involve development of model-based cancellation compensation for biodynamic feedthrough, based on experiments with a seated operator controlling a single degree-of-freedom moveable platform. The first addresses the uncertainty in the human operator's dynamics by developing a different model for each operator [32]. The second addresses model uncertainties by developing a mu-synthesis based controller [31]. One patent describes an actuated 'biodynamic resistant control stick' developed for aircraft control, which actively varies the magnitude and direction of the aircraft joystick's spring return force as a function of the motion of the aircraft [26].

Two publications present preliminary studies on biodynamic feedthrough in the HEnRE system. The first paper presents a system model showing the effects of the biodynamic feedthrough, with models for each of the major dynamic components, including the human body, with parameters specific to the HEnRE hardware. It illustrates the instability resulting from the biodynamic feedthrough [12]. A second paper presents a few simple controller-based approaches for reducing cab acceleration, as well as some ideas for more advanced state feedback control methods using the cab acceleration measurement as feedback [11]. A third paper discusses controller design and hardware testing results in terms of cylinder tracking performance and vibration

reduction [13].

2.3 Vibration Control

The approach taken in this research for minimizing biodynamic feedthrough is focused on reducing cab motion. One method used in this study is active vibration control using measurement of cab acceleration. Numerous publications over the past several decades involve a wide range of active vibration control designs for minimization of cab motion in vehicles, primarily for ergonomic purposes; these include automobiles, trains, off-road military vehicles, and mobile hydraulic equipment. For example, one simulation study uses a sky-hook damping approach with actuated suspension for vibration control of a quarter car model. This study compares a semi-active approach to a fully-active linear quadratic regulator (LQR) optimal controller [10]. Rahmfeld and Ivantysynova present a review paper that discusses various forms of passive, semi-active and active vibration control for mobile hydraulic equipment structures. These include vibration damping by force control, pressure control, velocity control and acceleration control. Some methods required additional hydraulic actuators, while others used the machine working hydraulics such as excavator or wheel loader arms. The actuators in such systems have dual functionality, both working and damping. The paper presents a comparison of methods in terms of sensors, electronic and hydraulic control methods, and energy use, but it does not provide a comparison of vibration damping performance [25].

In [36] and [35], active cab motion reduction for a wheel loader is achieved using an LQR-based state feedback controller. In this work, the working implement does have dual functionality, but it serves each purpose at different times during operation; it serves as a vibration damping component only while the machine is driving across rough terrain, and it serves only as a working implement when the machine is stationary. Pump control is used for the implement, which is implemented as an inner

feedback loop, along with an outer LQR-based state feedback controller which uses cab velocity as feedback. Cab velocity is approximated by integrating a cab acceleration measurement in real time. This produces a force on the cab that is proportional to and opposing cab velocity, producing an effect know in literature as 'sky-hook damping'. Another study implements active vibration control of an agricultural tractor with a spray boom. In this case, a problem arises when the tractor structural oscillations cause large motion of the boom tip. Accelerometers are mounted on the boom, and additional actuators are added to the cab to reduce those boom vibrations. The $H\infty$ controller design method is used on the spray boom [2].

Control of flexible robotic arms, and other machines exhibiting flexibility such as cranes, are also related problems. Some of the types of controller solutions used in such research problems can also be applied to the problem of backhoe cab vibration control. For instance, several variations of feedforward command generation, e.g. input shaping, command shaping and the OAT filter ([30], [29], [23], [28], [4]). A number of feedback control methods, such as Kalman filtering, have also been applied to reduce undesirable vibrations in systems with flexible links and flexible manipulators [33].

CHAPTER III

MODELING OF BIODYNAMIC FEEDTHROUGH

3.1 Modeling Overview

The first goal of this research is to investigate and improve our understanding of how biodynamic feedthrough affects the backhoe control system. Biodynamic feedthrough adds an additional feedback component to the traditional backhoe manual control system; therefore, a dynamic model of this complete system, including biodynamic feedthrough, is needed. In addition, the first step in the design of a compensating controller is to develop accurate models of the system dynamics. While it is preferable that the developed biodynamic feedthrough compensating controller design techniques be generalizable to a range of machine types, the first goal is to mitigate these undesirable effects on the HEnRE testbed. The model should be primarily first-principles-based for the purpose of generalizability, but it must also correlate well with the HEnRE system.

The component models were developed based on a hybrid of first principles and system identification. Purely first principles based models would be very complicated and include many forms of nonlinearities, which may or may not be significant in the overall system response. However, black-box system identification would also be undesirable in this case, since it would not provide much insight into the system dynamics and would make the results less generalizable to other systems. A wide range of nonlinear effects are present in these types of physical systems, in particular those involving hydraulics and high degree-of-freedom kinematics. Some of these effects were identified and modeled and are described in a later section. Addition of these nonlinearities to the simulations did not prove to improve the model correlation with

hardware results. The final controller designs are developed based on purely linear models. The biodynamic feedthrough system is divided into four main components, each of which are modeled separately. The system is shown in Fig. 8.

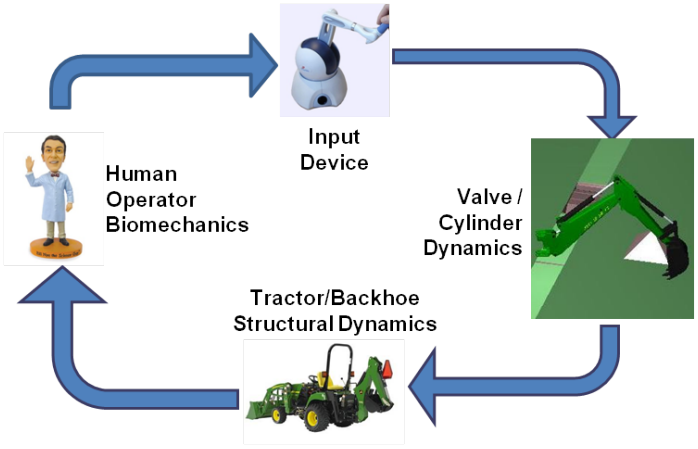

Figure 8: Main dynamic components

The backhoe control system with biodynamic feedthrough is a very high degree-of-freedom, complex system; for the purpose of reducing the dynamic system to a more manageable level of complexity, only fore-aft motion is considered throughout the system. While the full HEnRE control system uses coordinated position control, this testing incorporates closed loop position control of only the boom (shoulder) joint. By appropriately positioning the backhoe arm and assuming small angle approximations, it can be assumed that the backhoe motion provides solely fore-aft excitation, as described in [12].

Initially, two arm configurations were considered and modeled, one excited by the stick and the other excited by the boom. Both produce primarily fore-aft structure excitation. These two configurations are shown in Fig. 9. The boom excited case produces significantly larger cab vibrations, so this case is used throughout this work.

To determine a model for each major dynamic component, transfer function models are obtained for each measurable input-output relation. The inherent mechanical dynamics of the SensAble Omni are neglected, since it is designed with very low

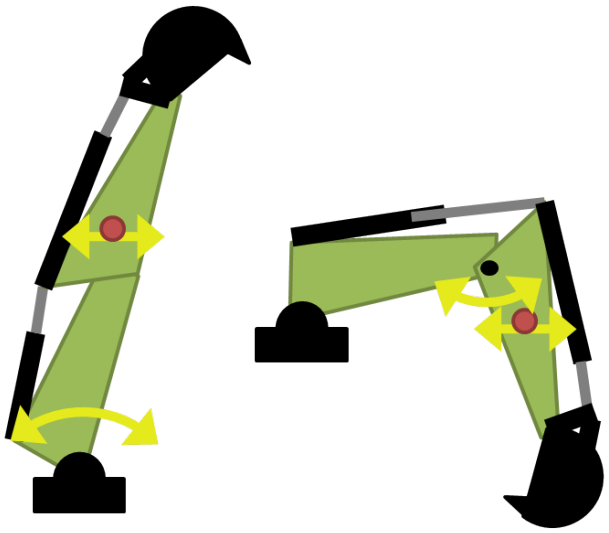

Figure 9: Two backhoe arm configurations producing primarily fore-aft structure excitation

inertia and little mechanical damping for the purposes of providing realistic haptic feedback. The force generating capability of the Omni could be used to modify its dynamics as needed to improve the performance of the system, but this approach is not tested in this research. The human body is modeled as transmissibility from seat motion to hand motion, with the body seated in a typical operating position. The tractor structure is similarly modeled as a mass-spring-damper system, with a transfer function corresponding to transmissibility from backhoe motion to seat motion.

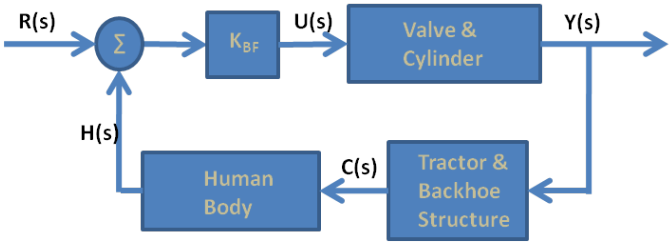

Figure 10: Basic biodynamic feedthrough block diagram

Figure 10 shows a block diagram of the system, incorporating these transfer functions. An appropriate transfer function is included to simulate the valve/cylinder dynamics, with a closed loop with PID controller used to achieve position-to-position mapping from Omni motion to cylinder motion. The position scale factor (K_{BF})

corresponds to the ratio of the workspace limits for the Omni and cylinder.

In order to decrease model complexity and match with measured data, model parameters and some parts of the transfer fucntion models used in this work are empirically determined. System identification by spectral analysis was peformed on three main components of the system: the valve/cylinder system, the backhoe/tractor structure, and the human body. The basic forms for the component models are developed based on first principles whenever possible, as described in [12] and [11].

Figure 8 shows how the main dynamic components relate. Hardware tests with software generated signals provided excitation for the purpose of system identification. Motion of the backhoe stick joint was used as excitation, from an external software input signal in the form of a chirp sine; measurements of cab acceleration and operator's hand motion are obtained. In the hardware, the following measurements are used for model development: (1) hand position relative to cab position, obtained from using the Omni, equipped with encoders, used as a measurement device rather than an input device, (2) cylinder position, measured using a linear position sensor, and (3) cab motion, measured using 3-axis MEMS accelerometers located at the operator's seat and at the Omni base.

Spectral analysis was used to obtain frequency response plots for each component. Bode plots and coherence plots are computed based on measured data, and frequency domain curve fits are used to determine transfer functions to match the measured data. Measurement data are often noisy and some have low input-to-output coherence, especially those using accelerometer measurements. Filtering and large data sets are used in order to mitigate these issues as much as possible, typically 15-25 data sets, each 40 seconds long with 1000 Hz sample rate. The measurement data sets are converted using Fourier transforms, then Eqn. 1 and Eqn. 2 are used to obtain the magnitude, phase and coherence relations between the input and output.

$$\hat{H}(f) = \frac{\hat{G}_{xy}(f)}{\hat{G}_{xx}(f)} \tag{1}$$

$$\gamma_{xy}^2(f) = \frac{\hat{G}_{xy}(f)^2}{\hat{G}_{xx}(f)\hat{G}_{yy}(f)} \tag{2}$$

where G_{xy} is the crosscorrelation between input and output, G_{xx} and G_{yy} are autocorrelations for the input and output, respectively, and γ_{xy} is the coherence. The magnitude and phase of $\hat{H}$ provide the Bode plots.

3.2 Valve and Cylinder Dynamics

In [8], a transfer function from input signal to flow rate is developed empirically for this particular valve, providing a basis for the development of the model for the valve/cylinder. It gives a third order transfer function from input valve signal to output flow rate, where one pole is at such high frequency that it can be neglected in this system. However, the addition of the backhoe arm and cylinder must be included. The dynamics of this lumped system vary with loading conditions and arm configuration, and they are different for each cylinder. Therefore, two separate models were obtained, one for the actuating joint for each of the two selected arm configurations.

In each case, the full valve/cylinder system is modeled as one lumped system with parameters determined from system identification. The input valve signal corresponds approximately to a commanded velocity, and the output cylinder position is measured, indicating that the desired transfer function from input valve signal to output cylinder position should be approximately third order with a free integrator. The integration effect, gravitational effects, and the difference in rod side and cap side pressures cause significant drift in open loop control; therefore, the data for system identification are obtained from within the closed position-to-position control loop. A chirp sine signal is used as input to the closed loop with PID controller. The valve control

signal, corresponding to the error signal inside the closed loop, is used as the input signal for system identification, and the cylinder position measurement is the output. Figure 11 shows Bode magnitude and phase plots comparing the valve/cylinder model and measured data for the boom-actuated arm configuration. Figure 12 shows the coherence.

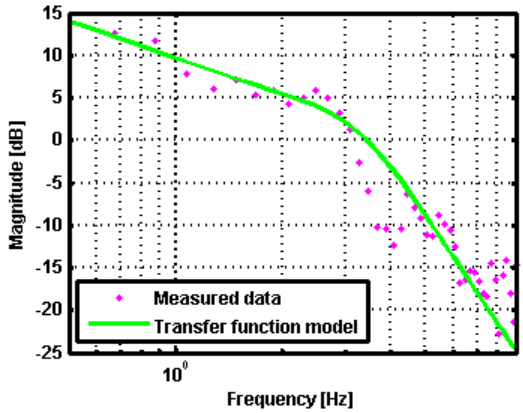

(a) Magnitude

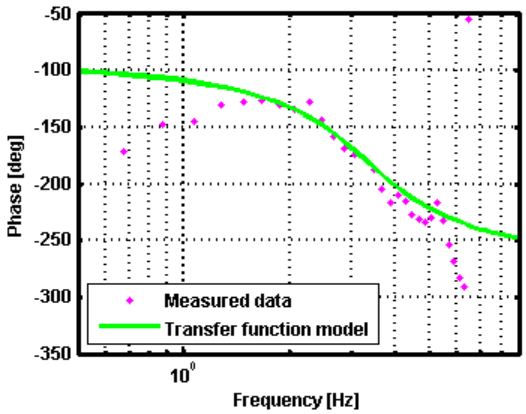

(b) Phase

Figure 11: Valve/cylinder Bode plot

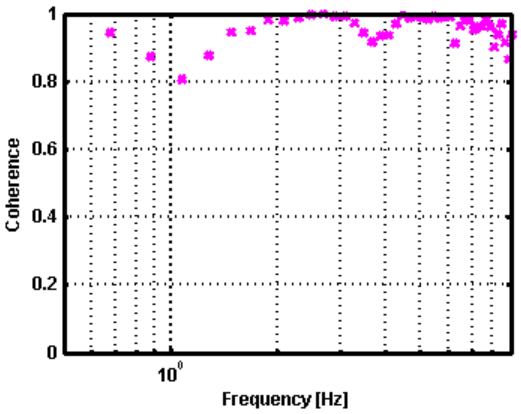

Figure 12: Valve/cylinder coherence

The empirically determined transfer function for the valve/cylinder component is given in 3. The parameters are also given in Eqn. 4.

$$\frac{Y(s)}{V(s)} = \frac{K_{VC} \cdot \omega_{nVC}^2}{s\left(s^2 + 2\zeta_{VC}\omega_{nVC} + \omega_{nVC}^2\right)} \tag{3}$$

$$\begin{aligned} K_{VC} &= 22.0 \\ \omega_{nVC} &= 21.2 \\ \zeta_{VC} &= 0.45 \end{aligned} \tag{4}$$

Backhoes have inherently low bandwidth This model matches well with measured data in the upper frequency range of interest, but the coherence begins to decrease below approximately 1 Hz. This nonlinear relation at low frequencies likely results from the effect of the valve deadband within the closed loop; at low frequencies, the error is small and likely to remain within the valve deadband. This nonlinearity is insignificant in the analysis of biodynamic feedthrough. It will be shown later that the biodynamic feedthrough has no significant effect at such low frequencies.

3.3 Tractor and Backhoe Structure Dynamics

A similar system identification analysis was performed on the tractor/backhoe structural dynamics. In this case, the form of the system model is based on a simple 2-mass-spring-damper system. For backhoes and excavators in operation, these structure dynamics vary depending on many factors, including the soil properties, the use of outriggers and front-end loaders for stability, and other external factors. They also vary significantly from one system to another. It is important to note that this analysis is based on the current HEnRE system setup, with the tractor mounted on steel stilts for convenience in testing, rather than sitting on its wheels. The stilts setup is most likely stiffer than the system sitting on wheels. Therefore, the cab acceleration generated from this setup is most likely lower amplitude and higher frequency than that of a more standard tractor placement. Acceleration was measured in two locations in the cab, at the base of the Omni and at the operator's seat. The measurements at both locations were very similar, indicating that the cab motion can be treated as a rigid body.

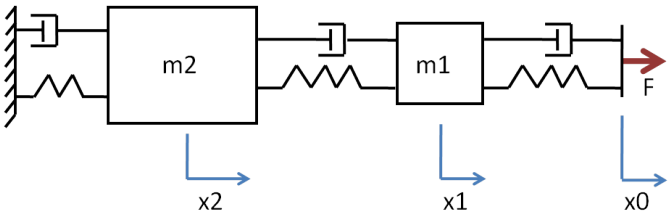

Figure 13: 2-Mass-spring-damper system representing lumped structure dynamics

Figure 13 shows the mass-spring-damper system upon which this model is based. It represents only the tractor structure. The two masses are used to represent two modes of this distributed system. The structure is attached to ground on one end and the cylinder actuator on the other. The applied force represents the force applied to the structure by the actuator, the actuator position is represented by x_0 and the cab position is represented by x_2. The model is a transfer function from cylinder position

Table 1: Structure Model Parameters for Boom Actuated Arm Configuration

K_S	0.45	ω_{nS1}	4.0	ζ_{S1}	0.06
		ω_{nS2}	6.2	ζ_{S2}	0.04

to cab position, plus two derivatives of cab position to account for the acceleration measurement at the cab. System identification cannot provide enough information to determine each unknown mass, spring and damping constant. Therefore, this transfer function was arranged such that the unknowns are lumped into frequency and damping terms that can be determined by system identification. Figure 14 shows the magnitude plot and model based on the measured data.

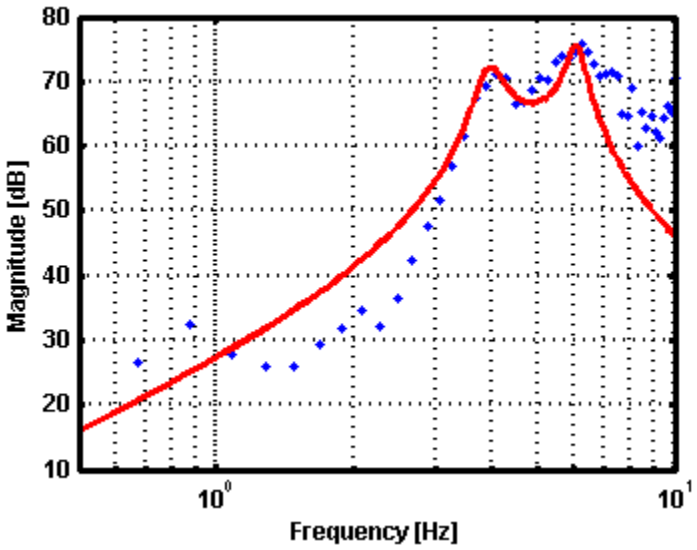

Figure 14: Structure dynamics magnitude plot

This gives an equation of the form in Eqn. 5, and the parameters are given in Table 1.

$$\frac{C(s)}{Y(s)} = K_S \cdot s^2 \cdot \frac{(2\zeta_{S1}\omega_{nS1} + \omega_{nS1}^2)}{(s^2 + 2\zeta_{S1}\omega_{nS1} + \omega_{nS1}^2)} \cdot \frac{(2\zeta_{S2}\omega_{nS2} + \omega_{nS2}^2)}{(s^2 + 2\zeta_{S2}\omega_{nS2} + \omega_{nS2}^2)} \tag{5}$$

These measurements have high coherence only in a small frequency range, near the natural frequencies of the structure. This structure has two large peaks near 5 Hz; the amplitudes of the measured acceleration at considerably lower or higher

frequencies are small, indicating that a small signal-to-noise ratio in these ranges is a likely contributor to the nonlinearities at frequencies above and below the structural modes. Simulation results show that biodynamic feedthrough occurs primarily in the frequency range near the natural frequencies of this structure; the smaller amplitude vibrations outside this frequency range are less significant.

3.4 Human Body Biomechanics

As in the case of the valve/cylinder and the structure, a linear transfer function model is developed to represent the human body dynamics using system identification. In this study, only nominal median male values for human body spring and damping parameters are considered; these parameters are expected to vary widely, and that parameter variation is a topic for future work. For the human model, data are obtained by two methods: 1) human subject trials, and 2) human body dynamic simulations using MSC.Adams and the add-on package LifeMOD.

The human body biomechanics are the most difficult component to model, and they are expected to vary significantly [14]. Many human body biomechanics models can be found in literature; however, in this case, the system involves a very specific case. The human body is in a seated position holding the input device in one hand, and the only two components of interest are the motion of the seat and the induced motion of the human hand. In terms of biodyanmic feedthrough, the body is considered to be a purely mechanical component; any cognitive or neuro-muscular effects are neglected.

In biodynamic feedthrough, the unwanted input resulting from the biodynamic feedthrough cannot be decoupled from the desired input. This creates difficulty in modeling the human body. Most commonly in the literature, as in this study, the unwanted input is approximated in a separate set of experiments in which the machine is excited externally, not by the human operator. In this system, the excitation is by

the backhoe stick motion, as for the other component measurements. The stick motion is commanded from an external software input, and the Omni input device is used for measurement rather than command. Human operators were seated in position for operation and instructed to hold the Omni as though operating the backhoe while the cab vibrated. This measured the Omni handle position with respect to the cab, giving a direct measurement of the unwanted Omni input as a function of backhoe motion. It should be noted that the original excitation signal is passed through the valve, cylinder and structure before exciting the human body. The cab vibration input to the human body can be measured in real-time, but this input excitation to the human body has significant variations in signal power and signal-to-noise ratio across the range of frequencies which may lead to some discrepancies in modeling. This test was performed on two human subjects.

LifeMOD is an add-on to the dynamics simulator MSC.Adams intended for modeling dynamics of the human body. This software is also used to model the vibration response of the human body, which provides more consistent results than human subject trials. This software allows the user to input body parameters such as overall height and weight, joint parameters, etc. From a set of user inputs, it can generate a set of 16 linkages and 18 joints with appropriately scaled masses, centers of mass, lengths, etc., to represent the human body, or the user can select median male or female parameters. Interactions with other bodies modeled in MSC.Adams can also be included. The user can input individual joint stiffnesses and damping coefficients, or use the values from the standard Hybrid III crash dummy, with a scale factor. Figure 15 shows an image of a human operator on the backhoe seat [22]. A LifeMOD model scaled to match the female test subject was used to obtain correlation between the LifeMOD simulation and human subject testing. The body is positioned such that the hand is placed at the nominal location of the Omni handle in the cab. The simulated operator is attached to the seat. A swept sine input is applied to the seat

in the fore-aft direction, and the response at the hand is recorded.

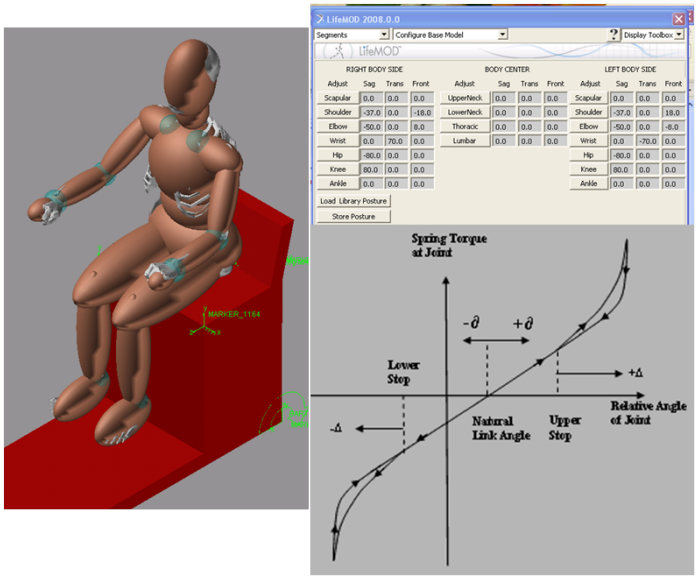

Figure 15: LifeMOD screenshots and joint hysteresis

Parameters for stiffness and damping of human body joints are variable and not well-known. In addition to variations from person to person, these values can vary significantly depending on joint angles and positions; in literature, these variations are sometimes modeled as ellipsoids, as discussed in [37]. They also vary depending on the activity level of the joint, as discussed in [37]; Jex and Magdaleno note a similar difference in biodynamic feedthrough depending on whether the operator is active or passive [14]. A number of research studies have investigated human body spring and damping parameters in various conditions, and results often vary by as much as an order of magnitude. Extensive testing on human body parameters is performed in the development and testing of the Hybrid III Crash Dummy [15]; these standard values, with a scale factor of 0.6 to account for a difference in activity level, are used in this analysis. This scale factor is determined based on values from similar sample LifeMOD simulations and by adjusting to match the frequency response of human test subject data. A comparison of magnitudes for input seat acceleration and output hand motion for two human test subjects, the median male LifeMOD model, and the

transfer function model is shown in Fig. 16.

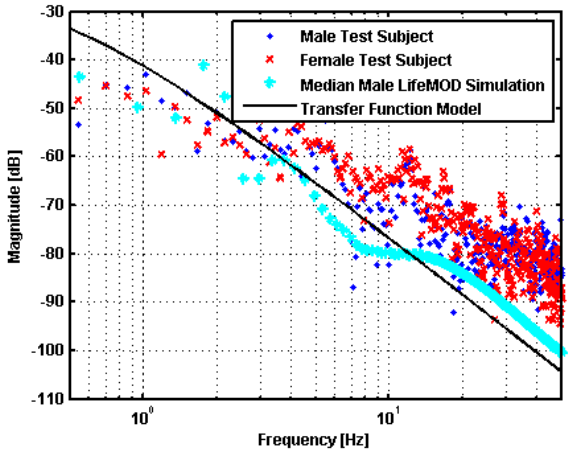

Figure 16: Human body dynamics magnitude plot, based on human subjects and simulation

The input signal for the human test subjects is an accelerometer measurement, which includes considerable noise, especially from motion induced by the running tractor motor. The transfer function model for the human body dynamics, with input seat acceleration and output hand motion, is given in Eqn. 6. The output hand motion is defined with respect to seat motion, not as an absolute position. The gain K_H is 0.56 mm/mm.

$$\frac{H(s)}{C(s)} = \frac{K_H}{s^2} \tag{6}$$

This human body model represents only a mass. While the human body is expected to be a flexible system, this model does not capture flexibility. The data show that the human body model is highly variable and, as expected, difficult to model. In the Bode magnitude plot, note that it is more important for the model to match the measurement data below approximately 10 Hz, since the dominant system dynamics are in this range. In the compensation methods to be discussed later, the goal is to minimize the input to this highly variable component, the human body. Therefore, the controller designs do not utilize this model. If the goal of minimizing excitation

of the human body can be achieved, then high model accuracy is not needed for the human.

Tests were performed to investigate the effect of varying the Omni position on biodynamic feedthrough. The same tests as described previously are performed with the Omni in three different positions, a nominal position, four inches forward from nominal, and four inches back from nominal, using one human test subject and the median male LifeMOD model. The results from the LifeMOD simulation are shown in Fig. 17. Position is varied only along the fore-aft axis.

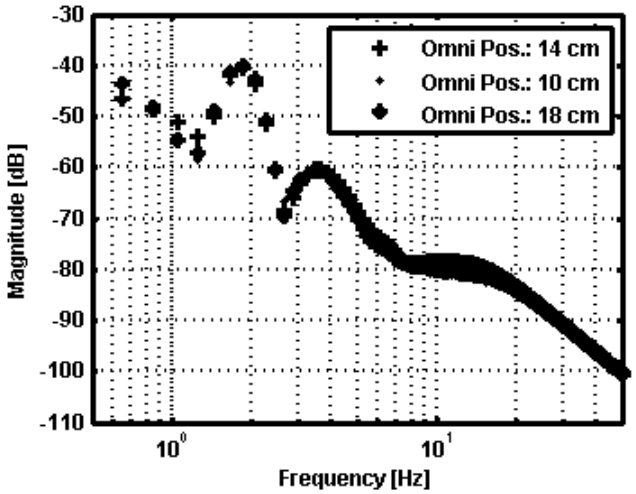

Figure 17: Variations in Omni position have little effect on human body response

A similar experiment was performed with one human operator, varying the Omni position. These results indicate that variation in Omni position with respect to the human body has little effect on vibration transmission into the input device.

CHAPTER IV

CONTROLLER DESIGN

4.1 Controller Design Overview

A number of methods for mitigating the biodynamic feedthrough effect have been considered. For a backhoe, it is desirable to develop a controller which mitigates this effect by reducing the cab vibration. The goal of the controller is to move the backhoe arm in such a way that the excitation of the flexible structure is minimized. This approach has added ergonomic benefits and does not require additional actuators. Several controller based methods are available for compensating for flexibility in motion control systems. These include both active and passive compensation strategies. Several forms of controllers are developed in this chapter.

In literature, these vibration compensating controllers are often studied in applications such as flexible robot arms, cranes and other machines in which the flexibility results in undesirable endpoint motion rather than base motion. Some references to flexible robot control were discussed in Chapter 2. Several methods, including filtering of structure natural frequencies, input shaping, and active compensation, are traditionally used to mitigate adverse effects of structural flexibility and vibration in such systems. These same general approaches can also be used to reduce structural vibration of the system's base, as in the case of the backhoe. However, Fig.18 illustrates a significant difference between flexible arm control and cab vibration reduction.

Consider two tracking control problems, one flexible arm control and one flexible base control, or backhoe cab vibration reduction. In the flexible arm control case, the goal is to track a reference position with x_1 using actuation force F. In this case, with a perfect model and knowledge of future inputs, the actuator position x_0 can make

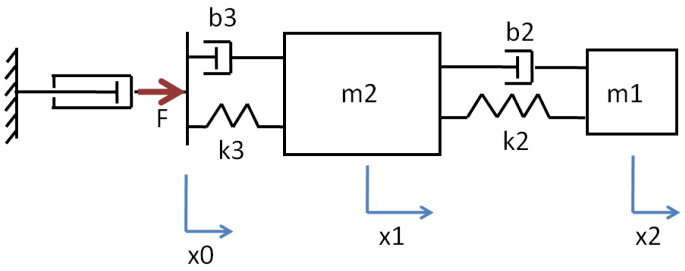

(a) Flexible arm control

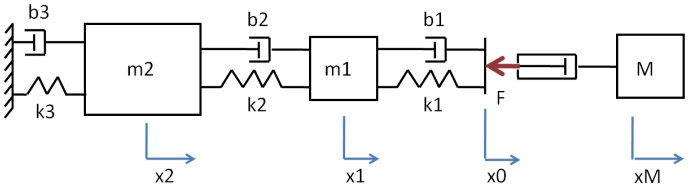

(b) Flexible base control

Figure 18: Flexible arm control and cab vibration control

any necessary motion to ensure that x_2 tracks the desired reference. The actuator has only one goal, to control x_2. Therefore, ideally, it is possible to obtain a control effort force F such that x_2 can perfectly track the reference.

In the case of the flexible base, the actuator has two conflicting goals, the first is to track a reference with x_M, and the second is to minimize motion of the structure, x_2 and x_1. This diagram represents a simplified, lumped-parameter linear system representing the flexible tractor/backhoe structure and the cylinder. The two-mass system represents the two modes of the structure, as described earlier. In this diagram, the cylinder actuator and a backhoe arm mass x_M are added. In this case, it is not possible to determine a control force F such that both goals are achieved perfectly. In all cases of controller designs for the case of the flexible base, there is a tradeoff between tracking performance, vibration reduction, and control effort.

The bandwidths of the system components are important in the compensation design for biodynamic feedthrough. Figure 19 shows Bode magnitude plots for each of the major components. First, note that most system components have poles or

zeros in the range of approximately 4-7 Hz, and these are within the operating frequency range. The structural dynamics are not considerably higher frequency, and they cannot simply be removed by a low-pass filter; this would significantly reduce the speed of response of the backhoe. It is desirable to reduce the effects of the structure flexible poles without making the backhoe response sluggish. Also, while the valve/cylinder system is generally slower than the structure dynamics, the cylinder response magnitude is not so diminished at the structure natural frequencies that it is unable cancel the structure natural frequencies.

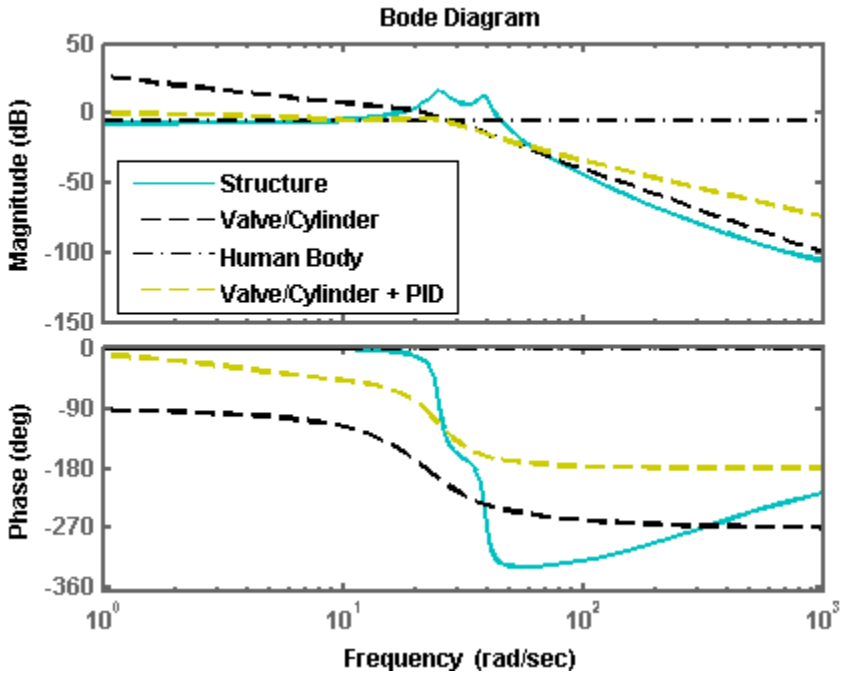

Figure 19: Bode diagram for each major dynamic component

One unique feature of the biodynamic feedthrough systems is that the reference input, or the operator's intended position command, and the biodynamic feedthrough signal, the operator's unwanted hand motion, cannot be decoupled. Therefore, the reference signal cannot be modified independent of the biodynamic feedback signal. Some techniques commonly applied to flexible motion systems, such as input shapers and notch filters, are typically applied as feedforward controllers and designed based

on the closed loop system. This approach allows for placement of zeros such that they reduce the effects of flexible poles. Since the reference signal cannot be separated from the feedback, such feedforward control cannot be applied outside the biodynamic feedthrough loop. However, these approaches may still be applied within the biodynamic feedthrough loop. If the biodynamic feedthrough gain K_{BF} is sufficiently small such that the closed loop poles remain close to the compensator zeros, then these control techniques may be designed based on the open loop system and still be effective. Figure 21 shows pole plots for two cases of the full system, one with the biodynamic feedthrough loop open and the other with that loop closed.

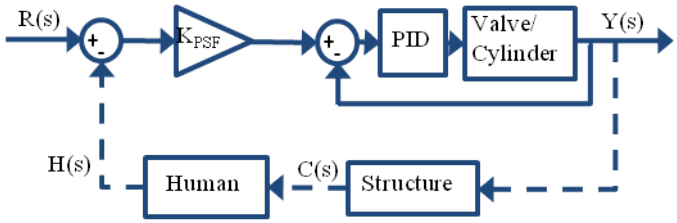

Figure 20: Biodynamic feedthrough block diagram with PID control

The pole plots in Fig. 21 show that the biodynamic feedthrough gain is relatively small and the closed loop poles are close to the open loop poles, in the case of this particular PID controlled system. While this cannot be generalized to all forms of controllers, since these closed loop pole locations depend on the controller, it does indicate that it may be sufficient to design the controllers based on the open loop system. It will be shown in a later section that these controller designs based on the open loop system do stabilize the model with biodynamic feedthrough.

Note that the PID-controlled system without vibration compensation is unstable; while the hardware/human system is not necessarily unstable, it does exhibit undesirable oscillations and limit cycling in some cases. In the linear models of the nonlinear hardware/human system, such limit cycling may appear as instability. Later results will show that the same compensation techniques that stabilize the linear model also

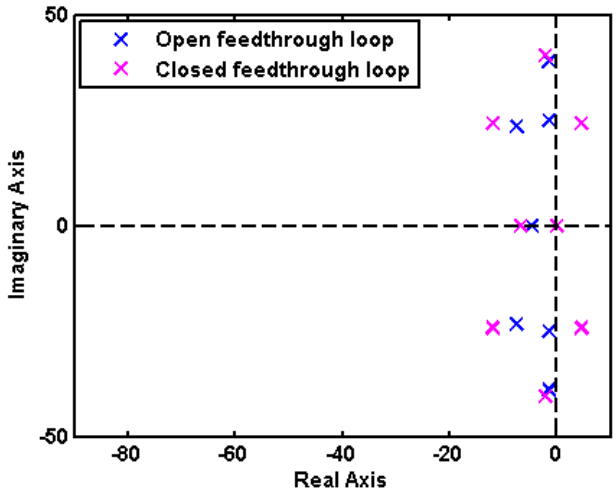

Figure 21: Pole plots for nominal PID-controlled system with open and closed biodynamic feedthrough loop

mitigate the biodynamic feedthrough effect in the hardware system.

The next sections discuss development of controllers based on the valve/cylinder and structure components only, with the goals of achieving good cylinder tracking performance while minimizing cab excitation; initially, the biodynamic feedthrough loop is neglected. These controllers will then be applied within the biodynamic feedthrough loop, and the stability will be analyzed.

4.2 Classical Compensation

Several different forms of classical and state-space controllers were developed and simulated in MATLAB/Simulink and tested in hardware, starting with the simplest and progressing to more complex. The goals for these controllers are to achieve adequate cylinder tracking performance while minimizing cab motion excitation. Two main approaches are presented, (1) a simple PID cylinder position controller with vibration compensation in the form of a notch filter at the structure natural frequency and an input shaper, and (2) an active vibration control approach using a state space controller.

4.2.1 Notch filter

Figure 22 shows a block diagram of the classical control system with the notch filter, including the inner cylinder control loop and the outer biodynamic feedthrough loop. Equation 7 gives the transfer function for the notch filter.

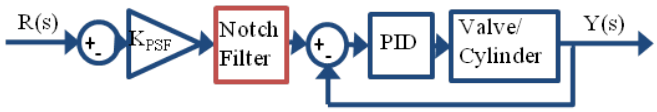

Figure 22: Classical block diagram

$$D_N = \frac{(s^2 + 2\zeta_N \omega_{nN} + \omega_{nN}^2)}{(s + \omega_{nN})^2} \tag{7}$$

The zeros of the filter are placed at a frequency midway between the two distinct natural frequencies of the structure at 4.0 Hz and 6.2 Hz, and the damping is tuned such that the desired magnitude reduction is obtained at both natural frequency peaks. The notch filter poles were placed at the same frequency as the zeros, but critically damped. The designer has some freedom in placing these poles; placing them too slow or too fast both have negative consequences. Others have determined that the frequency of the zeros achieves an appropriate balance [9]. Note that the filter is inside the biodynamic feedthrough loop but outside the valve feedback control loop.

The notch filter has the advantage of simplicity, but it does not utilize the measured cab vibration as feedback, so it does not provide disturbance rejection or compensate for any unmodeled cab motion. An adaptive notch filter which varies the center frequency based on variations in structure parameters is one possibility for future work.

4.2.2 Input shaper

The input shaper is a common method of compensating for flexibility in motion control systems. It has the advantage of design simplicity, and it tends to be effective at cancelling vibrations. The concept of the input shaper is to take the command at each instant, divide it into segments, and delay some of the segments such that they cancel the vibration of the machine induced by the first segment. However, it introduces some time delay, which can be problematic in terms of stability when it is included inside a feedback loop. It will be shown in a later section that the time delay induced by the input shaper in this system does not produce instability, however.

As with the notch filter, the goal of the input shaper is to reduce the structural vibrations. The poles associated with the tractor structure are very lightly damped; therefore, it is sufficient to assume zero damping in the design of the input shaper. Several forms of input shapers are available. In general, the more robust input shaper designs add more time delay. Because this input shaper is added inside the biodynamic feedthrough feedback loop, it was desirable to minimize the time delay. Therefore, a ZV, or zero vibration, shaper was selected.

The structure has two distinct natural frequencies in the frequency range of interest for this system. A two-mode ZV shaper was used to cancel both of these natural frequencies. an alternative design would be to use a single-mode ZVD or EI input shaper at a frequency between the two natural frequencies; this is a possibility for future work [30].

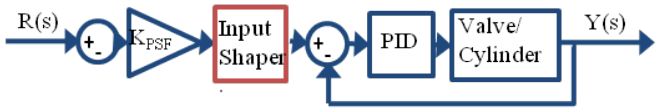

Figure 23: Classical block diagram

The basic equations for a single-mode ZV input shaper are given in (8) and (9). The component that is added to the block diagram shown in Fig. 23 is given by $I(s)$.

The single-mode equations describe two impulses of equal magnitude, with the second occurring at half of the period of the structure oscillation. The impulse amplitudes are denoted by A_i and corresponding time delays are denoted by t_i. A more complete development of the ZV input shaper design is given in [30].

$$I_1(s) = A_1 + A_2 \cdot e^{t_1 s} \qquad t_1 = \frac{\pi}{\omega_d} \tag{8}$$

$$\begin{bmatrix} A_i \\ t_i \end{bmatrix} = \begin{bmatrix} 0.5 & 0.5 \\ 0 & t_1 \end{bmatrix} \tag{9}$$

In order to add a second mode to the shaper design, two ZV input shapers are convolved as in Eqn. 10, which corresponds to multiplication in the Laplace domain. The subscripts on time delays t_1 and t_2 denote the parameters for a single-mode input shaper at that natural frequency. This convolution results in a matrix of impulse amplitudes A_i and corresponding time delays t_i given in Eqn. 11.

$$I(s) = I_1(s) \cdot I_2(s) \tag{10}$$

$$\begin{bmatrix} A_i \\ t_i \end{bmatrix} = \begin{bmatrix} 0.25 & 0.25 & 0.25 & 0.25 \\ 0 & t_1 & t_2 & t_1 + t_2 \end{bmatrix} \tag{11}$$

An alternative strategy would be to use a single more robust single-mode ZVD or EI input shaper (see [30]) at a frequency between the two natural frequencies; this is a possibility for future work. This input shaper design results in a total time delay of 0.2 seconds.

4.3 State Space Controller Design

While the previous methods provided passive compensation for cab vibration, another control strategy for cab vibration reduction is to utilize the measured cab acceleration as feedback, and to actively cancel that measured vibration. This approach

is implemented as a full state feedback optimal Linear Quadratic Regulator (LQR), and it uses the working implement for active vibration compensation. This has the advantage of providing some disturbance rejection and compensation for unmodeled structural vibrations.

This section describes the development of two types of active cab vibration compensation, using full state feedback control, cab acceleration feedback and cab velocity feedback. The two approaches have the same controller structure. In active damping, the compensator and actuator provide a force opposing cab velocity; this approach uses measured cab velocity as feedback.

4.3.1 Controller development with active compensation

The first step in designing a state space controller is to obtain a state space model of the system. This model can be easily obtained from the transfer functions described in Chapter 3. This model includes the valve/cylinder component and the tractor/backhoe structure component. The human body is not included in the system for several reasons. Aside from the human body dynamics being highly variable, including the human body dynamics in the state space system creates other difficulties in compensator design. The unwanted hand motion of the human body cannot be measured, since it cannot be decoupled from the input. As a result, addition of the human body model to the state space system model makes the model neither completeley observable nor completely controllable. Therefore, the system to be controlled includes only the valve/cylinder and tractor/backhoe structure.

In general, state space controllers require accurate system models. In this system, the valve/cylinder response in this structural configuration has significant nonlinear effects, resulting from unequal piston-side and rod-side areas, gravitational effects, cylinder stiction, valve deadband and saturation, and others. Feedback linearization and other nonlinear control techniques could be applied to compensate for these. A

simpler method to achieve more linear response from the hydraulic cylinder, though possibly less effective, is to include an inner proportional-only cylinder velocity control loop. This improved the linearity of the cylinder response. Then state feedback control was applied external to this velocity-controlled cylinder. Only cylinder position is measured; therefore, the cylinder measurement must be differentiated to provide the desired cylinder velocity feedback. The cylinder position measurement is sufficiently smooth that this differentiation, after low-pass filtering, provides meaningful feedback. Fig. 24 shows this inner velocity feedback loop.

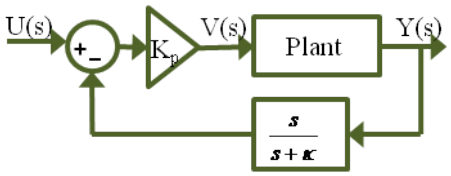

Figure 24: Inner cylinder velocity feedback loop

The closed loop transfer function for the valve/cylinder dynamics with proportional velocity feedback is given in Eqn. 12.

$$\frac{Y(s)}{U(s)} = \frac{K_P K_{VC} \omega_{nVC}^2}{s(s^2 + 2\zeta_{VC}\omega_{nVC}s + \omega_{nVC}^2 + KK\omega_{nVC}^2)} \tag{12}$$

This valve/cylinder model with proportional velocity control (Eqn. 12) is combined with the structural dynamics model (Eqn. 5) to produce a single-input, two-output state space system. The two outputs are the cylinder position and cab acceleration, both of which are measured in the hardware system.

The input reference valve velocity is denoted by $U(s)$, and the measurements are denoted by cylinder position $Y(s)$ and cab acceleration ($s^2C(s)$). This full state feedback system is shown in Fig. 25, excluding the human model and biodynamic feedthrough feedback loop.

The controller has two conflicting objectives, to reduce cab motion and drive cylinder position to a reference. This makes the LQR optimal control method a suitable choice for selecting the state feedback gains. This method allows the designer

to choose weights to vary the tradeoffs between control effort and performance, as well as the tradeoffs between individual states.

The next step is to determine the controller gains. The cost function for the LQR optimization is given by

$$J = \int_0^\infty \left(x^T Q_{LQR} x + u^T R_{LQR} u \right) dt \tag{13}$$

where x the state vector, u is the control signal, and Q_{LQR} and R_{LQR} are weighting matrices. The relative values between Q_{LQR} and R_{LQR} determine the tradeoff between performance and control effort, while the values within the Q_{LQR} matrix determine the tradeoff between the individual states. In order to apply weights to the individual outputs rather than individual states, we use an additional weighting matrix Λ, as shown in Eqn. 14.

$$\Lambda = \begin{bmatrix} \alpha & 0 \\ 0 & \beta \end{bmatrix} \tag{14}$$

The term α is a weight for the cylinder position output, and the term β is a weight for the cab acceleration output. This matrix and the output matrix C are used to determine Q_{LQR}.

$$R_{LQR} = 1, \quad Q_{LQR} = \left[(\Lambda C)^T (\Lambda C) \right] \tag{15}$$

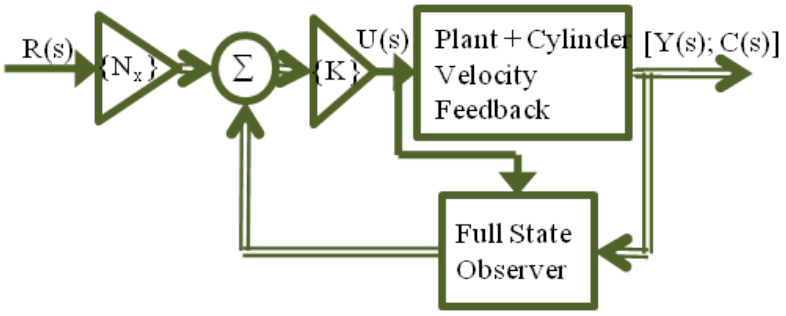

Figure 25: State space block diagram with inner cylinder velocity feedback

From this LQR optimization, the optimal feedback gain matrix K is determined based on the well-known matrix Ricatti equation (16), or by the $lqr(*)$ function in MATLAB. The terms α and β were determined by (a) finding a rough approximation of reasonable values from Simulink simulation testing, and (b) optimized by a coarse pattern search, by testing the controller on the hardware for several possible combinations of gains.

$$A^T S + SA - (SB + N)R^{-1}(B^T S + N)^T + Q = 0, \quad N = 0 \tag{16}$$

The $\bar{N}$ method described in [9] is used to introduce the cylinder position reference signal. The equations provide gains applied to control effort and added to the states. In this case, the reference term added to control effort N_u is zero, and the reference multiplied by N_x is added to the states.

$$\begin{bmatrix} N_x \\ N_u \end{bmatrix} = \begin{bmatrix} A & B \\ C & D \end{bmatrix}^{-1} \cdot \begin{bmatrix} 0 \\ 1 \end{bmatrix}, \qquad N_u = 0 \tag{17}$$

The system is represented in state space form by the standard convention of A, B, C and D matrices. The system has 7 states, with only two measurable, so an observer is needed. A full state Luenberger observer is used. The system is completely observable, and the gains were determined using pole placement. The observer poles were chosen to be approximately 4 to 5 times the frequency of the system poles and all real. The measurement signals were filtered using an analog low-pass filter followed by a second digital low-pass filter. The system outputs are two of the states, so the observer outputs could be easily validated. In spite of the noisy accelerometer measurement, the observer outputs tracked the corresponding measurements well.

4.3.2 Active vibration compensation by cab velocity feedback

One modification to this state space active vibration compensation approach proved to improve the system performance. A number of variations on this LQR controller were tested both in hardware and simulation. The best results were achieved from the cab velocity feedback approach, rather than cab acceleration feedback. Active damping is obtained by feeding back cab velocity rather than cab acceleration; cab velocity is obtained by integrating the measured cab acceleration signal in real time. This integration has a smoothing effect on the inherently noisy acceleration measurement. This approach uses the same controller structure, same observer, and same methods for computing gains. The only difference is the system output.

The integration in the hardware system is achieved using an approximate integrator, or a pole that is much slower than the system dynamics, rather than a pure integrator; this helps to reduce drift that occurs from integrating a noisy signal. A high pass filter is also used to eliminate any DC offset from the accelerometer signal.

4.4 Stability with Biodynamic Feedthrough

All of the controllers described in this chapter were designed based on an open biodynamic feedthrough loop. It is important to show that they are stable with the biodynamic feedthrough. The next two sections show that all of the applied controllers do create stable systems when the biodynamic feedthrough loop is added, with the nominal biodynamic feedthrough gain K_{BF}.

4.4.1 Stability with notch filter and input shaper

The full system model with PID controller and nominal parameters, including biodynamic feedthrough and no cab vibration compensation, is unstable. The hardware system is not necessarily unstable, but it exhibits undesirable oscillations and limit cycling with the operator on the tractor. The physical system has a variety of

nonlinearities, which are not included in this model; these nonlinear effects such as limit cycling may appear as instability in the linear model. The input shaper adds a set of time delays to the system, inside a feedback loop. It is desirable for the vibration compensators to stabilize the linear models; the effects which stabilize this model are expected to also improve response of the physical system with biodynamic feedthrough.

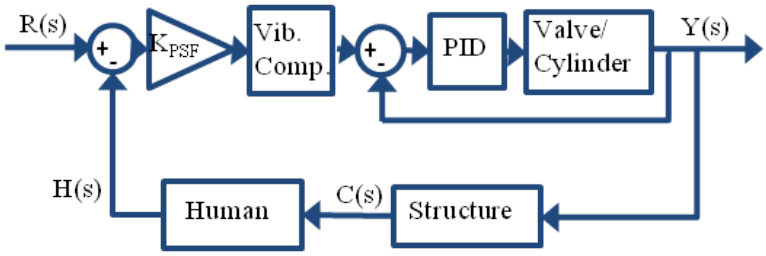

Figure 26: PID controllers with biodynamic feedthrough

Figure 26 shows the classical block diagram with biodynamic feedthrough. Either the notch filter or the input shaper, or neither, is included in the block titled "Vib. Comp.". The input shaper adds time delays inside the feedback loop; therefore, it is not sufficient to simply check that the poles of the system are in the left half-plane. One test for stability that is more appropriate with time delay is the Nyquist Stability Criterion. It requires that the number of encirclements of the point -1 in the Nyquist plot of the open loop system plus the number of unstable open loop poles is equal to zero, in order for the system to be stable. None of the open loop systems contain any unstable poles; therefore, the Nyquist plot must not encircle -1. In order to compare with the input shaper, the Nyquist criterion is also used to analyze stability of the nominal uncompensated system and the system with notch filter. The Nyquist plots shown in Fig. 27 are for the full systems, including the human body dynamics, but with the biodynamic feedthrough loop open.

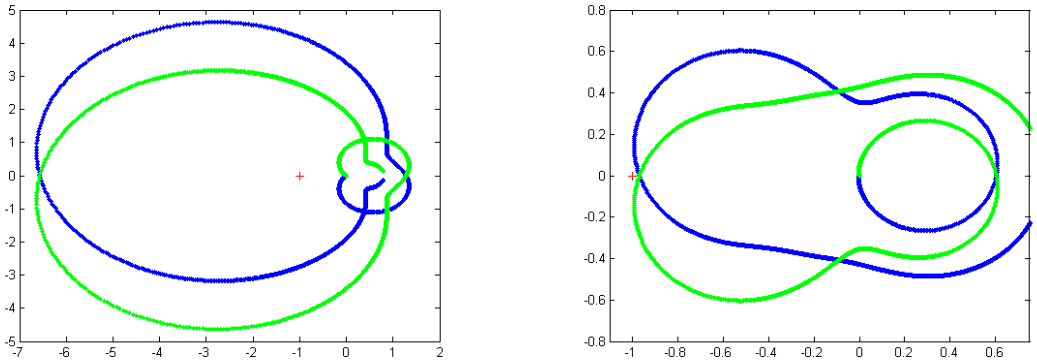

(a) No vibration compensation

(b) Notch Filter

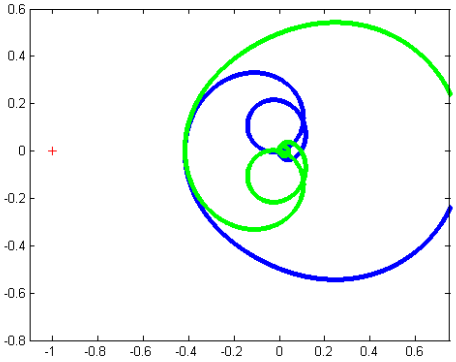

(c) Input Shaper

Figure 27: Nyquist plots for system with biodynamic feedthrough, 3 types of controllers

The Nyquist plot for the nominal system, or the system without vibration compensation, shows two clockwise encirclements of -1, indicating the instability. The plot for the notch filtered system does not encircle -1, indicating stability; however, a slight increase in the biodynamic feedthrough gain would lead to an unstable model. The system with the input shaper also does not encircle -1, proving that the closed loop system with the input shaper inside the biodynamic feedthrough loop is stable, in spite of the time delays.

It should be noted that any added vibration compensation treatment which increases phase lag would tend to have a destabilizing effect. However, that is not the case for the input shaper and notch filter in this system. In the case of the input shaper, as discussed before, this phase shift takes the form of a time delay. In the case of the notch filter, the phase shift is a lag. These filters also have the effect of reducing the magnitude near the point where the phase reaches -180 degrees. Both the notch filter and input shaper are able to sufficiently reduce the magnitude to stabilize the system. As shown in the Nyquist plots, both compensators reduce the magnitude to less than unity at a phase angle of -180 degrees.

4.4.2 Stability of state space controllers

The next step is to prove stability for the state space controllers. These systems do not include time delays. In these cases, the simplest method to prove stability is to show that the closed loop poles are in the left half-plane. Figure 28 shows the state space system with the biodynamic feedthrough loop added.

In order to determine the system poles, we must first determine the full state space system model. The system has two outputs, cylinder position and cab acceleration. However, the choice of inputs and outputs is irrelevant in the stability analysis. Therefore, the C matrix used for the full system includes only the cab acceleration as feedback, since that is the only signal that goes into the biodynamic feedthrough.

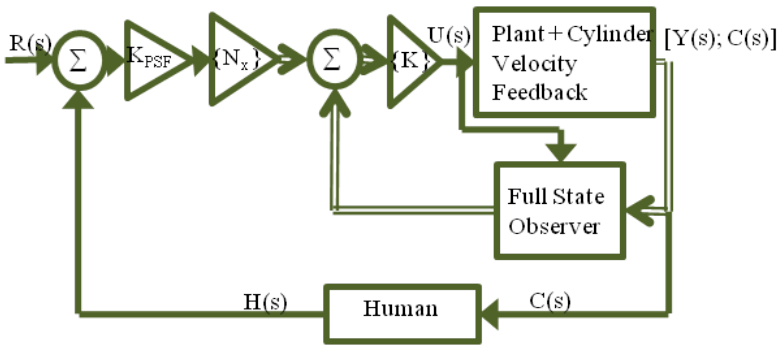

Figure 28: State space control with biodynamic feedthrough

This reduces the full state space system to a single-input-single-output system, which can be described by a single transfer function. Equation 18 indicates the original C matrix components, and the equations for the full state space system, excluding biodynamic feedthrough, are given in (19).

$$C = \begin{bmatrix} C_{CYL} \\ C_{CAB} \end{bmatrix} \tag{18}$$

$$\begin{aligned} A_{FULL} &= \begin{bmatrix} A - BK & -BK \\ 0 & A - LC \end{bmatrix} \qquad B_{FULL} = \begin{bmatrix} B \\ B \end{bmatrix} \\ C_{FULL} &= \begin{bmatrix} C_{CAB} \\ 0 \end{bmatrix} \qquad D_{FULL} = [0] \end{aligned} \tag{19}$$

Once this system is reduced to a transfer function, the full closed loop system transfer function, with feedback through the human body and the biodynamic feedthrough gain K_{BF}, can be computed. This calculation was done for each of the three types of state space controllers, one with no cab vibration compensation, one with cab acceleration feedback and one with cab velocity feedback. The resulting pole locations are shown in Table 2. The system models are stable in all three cases.

These controllers are implemented both in simulation and in hardware, and results are given in the following sections.

Table 2: Poles of State Space Systems with Biodynamic Feedthrough

No Vibration Compensation	Cab Acceleration Feedback	Cab Velocity Feedback
0.00	0.00	0.00
-7.51	-7.51	-7.43
-1.51 -25.09i	-1.87 -25.04i	-9.49 -22.95i
-1.51 +25.09i	-1.87 +25.04i	-9.49 +22.95i
-10.18 -23.25i	-10.14 -23.27i	-4.86 -25.19i
-10.18 +23.25i	-10.14 +23.27i	-4.86 +25.19i
-1.56 -38.92i	-1.63 -38.96i	-1.92 -39.14i
-1.56 +38.92i	-1.63 +38.96i	-1.92 +39.14i
-175.00	-175.00	-175.00
-176.00	-176.00	-176.00
-180.00	-180.00	-180.00
-190.01	-190.00	-190.00
-190.99	-191.00	-191.00
-195.00	-195.00	-195.00
-196.00	-196.00	-196.00

CHAPTER V

VIBRATION COMPENSATION EXPERIMENTS

5.1 Vibration Compensation Overview

The first goal of this research is to develop controllers which excite minimal cab vibration while still providing adequate cylinder tracking performance. This chapter describes a set of experiments to evaluate each of the controller designs developed in Chapter 4, with respect to tracking performance and reduction of cab vibration. These experiments use only the tractor/backhoe system; the human is omitted, so the biodynamic feedthrough is removed from the system. The inputs in each case are software generated cylinder command signals. The results show comparisons of the performance of the controllers in terms of two system outputs: cylinder tracking and cab vibration. Similar experiments are performed both in simulation, using the models developed in Chapter 3, and in the hardware system. They consider only the backhoe system, with the human in the loop neglected; the next chapter describes a set of human operator experiments.

These experiments are intended to demonstrate how several forms of controllers can be used to reduce cab vibration. They are not necessarily intended to determine which is the best controller type based on this set of performance results, since some controller types require different forms of parameter tuning, and they are not necessarily tuned in a manner that provides a fair comparison. For each controller type, the cab vibration compensation results in some form of degradation of cylinder tracking performance; for different controller types, this degradation manifests in different ways. For instance, in the case of the input shaper, this performance degradation is in the form of a lag in response; in the case of the active LQR compensators, the most noticeable problem is the higher frequency shakiness in the cylinder response resulting from the motions intended to cancel cab vibration. It is important to note that the development of these controllers often involves a tradeoff between tracking performance and vibration reduction, and in some cases, the balance of this tradeoff is determined by the designer. The clearest example of this balance is the LQR

controller design; in which the designer directly sets the weights for each output, corresponding to cylinder position tracking and cab vibration, and for the balance between control effort and overall performance. For the notch filter, the designer can tune the magnitude of vibration reduction at the desired frequency and the range of frequencies by tuning the damping on the filter zeros. For the controller designs tested in these experiments, the parameters associated with these design tradeoffs are not optimized; in general, they were tuned manually in hardware experiments. In the case of LQR control, a very coarse pattern search optimization was used to determine appropriate weighting parameters. A direct comparison of the different controller design techniques with optimized parameters is a possibility for future work.

The following sections give results for experiments with two types of software generated inputs: a swept sine signal and a slowly varying trapezoidal signal. The inputs are cylinder position reference signals, given to the closed loop cylinder controllers. The trapezoidal position signal was generated by integrating a trapezoidal velocity profile; this provides the general shape of a trapezoid, but with smooth corners. The trapezoidal signal is slowly varying and larger amplitude. This slowly varying signal is intended to demonstrate the controllers' tracking performance; it excites only very small cab vibration, and it does not demonstrate the controllers' abilities to cancel cab vibration. The swept sine signal is generally much more aggressive, quickly varying, and smaller amplitude. This input excites large cab vibrations, but at the higher frequencies, it is beyond the frequency range that the cylinder can track well. This more aggressive signal is primarily intended to demonstrate the controllers' abilities to reduce cab vibration, and it makes a more obvious indication of the vibration reduction and the frequencies affected. Similar experiments were performed both in Simulink simulations and in hardware.

5.2 PID Control Simulations

This section describes the simulation performance of three cases based on classical control techniques. All three cases use the same PID controller for closed loop position control of the valve/cylinder. This PID controller was tuned using the Ziegler-Nichols method. One case includes no cab vibration compensation; this controller is intended to be a benchmark to compare the performance of two forms of cab vibration compensation. For the other two cases, two types of vibration compensation are added, a notch filter and a ZV input shaper.

Figure 29 shows simulation response to a cylinder position reference input of a swept sine signal. The swept sine signal varies linearly with frequency; as time increases, frequency increases. The frequency range is 0.01 Hz to 8 Hz.

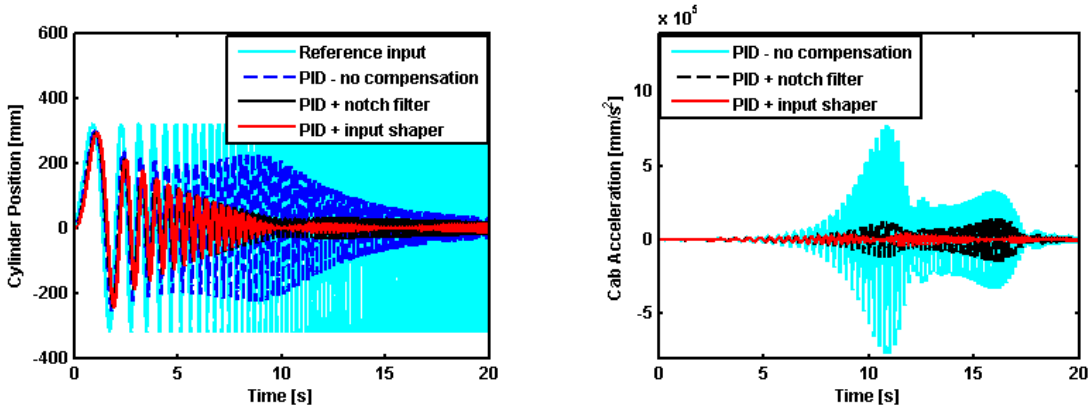

(a) Cylinder position

(b) Cab acceleration

Figure 29: Simulated response to swept sine input - PID controllers

The cylinder response plot shows that the addition of the notch filter and input shaper do cause a decrease in output cylinder position magnitude, particularly at frequencies near the structure natural frequencies. This reduction happens to be near the corner frequency of the uncompensated PID controlled system. The addition of these compensators does result in decreased bandwidth of the cylinder response. The cab acceleration plots show a large reduction in cab vibration with this type of input, especially using the input shaper. Note that the horizontal axis corresponds to time;

it also corresponds to frequency, since frequency varies linearly with time. The two peaks in cab acceleration correspond to two natural frequencies of the structure.

Figure 30 shows simulation response of the same three systems to a smoothed-trapezoidal input. This repeating signal has a cycle rate of 0.167 Hz. For this slowly varying reference signal, the input excites much smaller cab vibrations. Both the input shaper and notch filter reduce cab acceleration considerably.

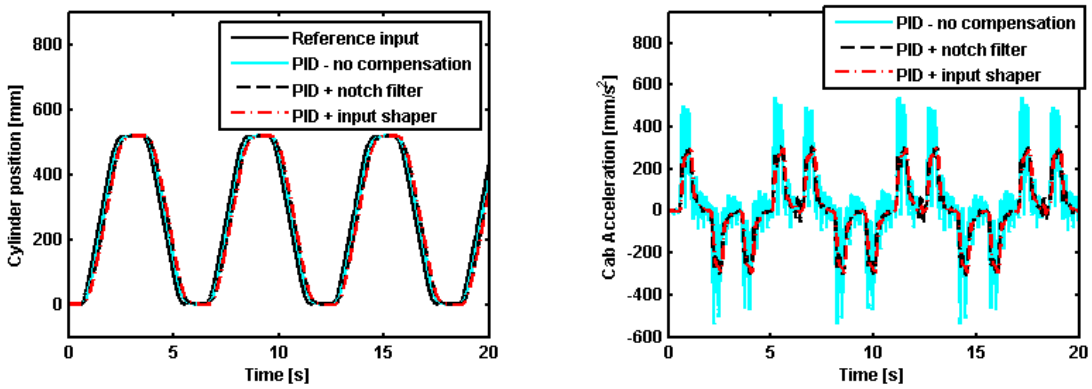

(a) Cylinder position

(b) Cab acceleration

Figure 30: Simulated response to trapezoidal input - PID controllers

In simulation, all of the controllers are able to track the trapezoidal input well, and both the input shaper and notch filter prove to significantly reduce cab vibration.

5.3 Active Compensation Simulations

This section compares results from three different forms of active compensation controllers, using LQR and state feedback. All three controllers have the same form; they have the same states, they all use full-state feedback and a full-state observer, and the same methods are used to determine gains. The only differences between these controllers are in which states are treated as measurement signals (or integration of the physical measurement) and in how those states are weighted in the Q_{LQR} matrix for determining controller gains. These controller developments are described in detail in Chapter 4.

Tuning is required for both the PID controller and the LQR-based controller. In order to determine the most appropriate gains for this system, the designer would need to consider the system including the human, with biodynamic feedthrough included. This would require human subject tests for the purposes of determining appropriate gains. This would most likely be an iterative process. Given the constraints on resources and time, consideratn of the human and biodynamic feedthrough in the tuning processes were excluded. The controllers were tuned based on performance with a software input. In the case of the PID controller, the Ziegler-Nichols tuning method was used for the system with no vibration compensation. These parameters were not changed when the input shaper and notch filter were added.

Tuning of the LQR controller includes the vibration compensation. First, the cylinder position weight α was increased until valve saturation occurred with the swept sine input. This provided the gain for the system without vibration compensation. Next, the cab vibration weight β was increased until substantial shakiness was visible in the cylinder response; this weight is highly subjective. The designer must choose some parameters. There is no exact way to achieve equivalent performance between the PID and LQR controllers, if it is possible. Therefore, the purpose of these tests is not to compare these two different types of controllers; it is to evaluate

the addition of vibration compensation with respect to the same controller type.

In one LQR controller case, only the cylinder position measurement is considered; zero weight is placed on the cab vibration states. This first case has zero compensation for cab vibration, so it is another benchmark LQR controller. In a second controller, the cab acceleration measurement is used as feedback and weighted appropriately in the determination of controller gains. Similarly, in a third controller, the cab velocity state is used as feedback. The same tests are performed as with the PID controllers, using a swept sine and trapezoidal input.

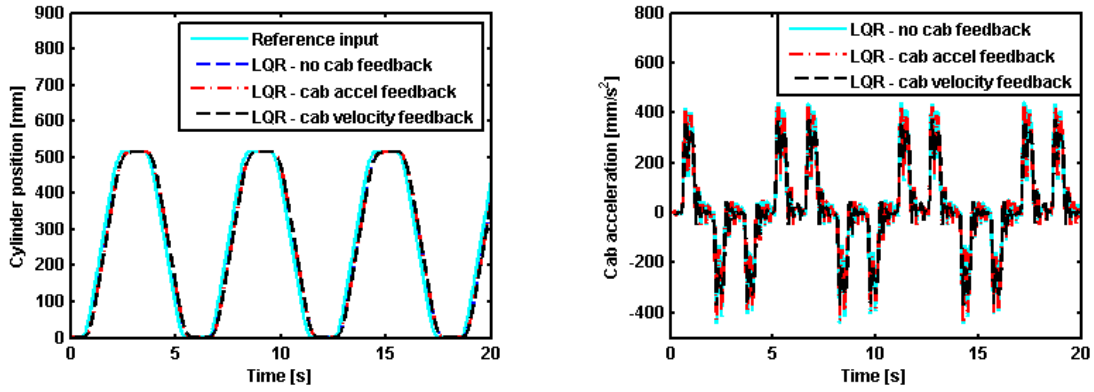

(a) Cylinder position

(b) Cab acceleration

Figure 31: Simulated response to trapezoidal input - LQR full state feedback controllers

Figure 5.3 shows the response of these three different LQR-based state feedback controllers to a smoothed-trapezoidal input. As in the case of the PID controllers, all versions provide adequate cylinder position tracking of this slowly varying signal. Only small cab vibrations are induced, and the controllers are able to eliminate only a small percentage of those.

Similarly, Fig. 32 shows simulated response to a swept sine input from 0.01 Hz to 8 Hz. The cab velocity feedback compensator provides significant cab vibration reduction, while the acceleration feedback compensator produces little reduction in cab vibration. In simulation, this results from the designer's choice of the weighting

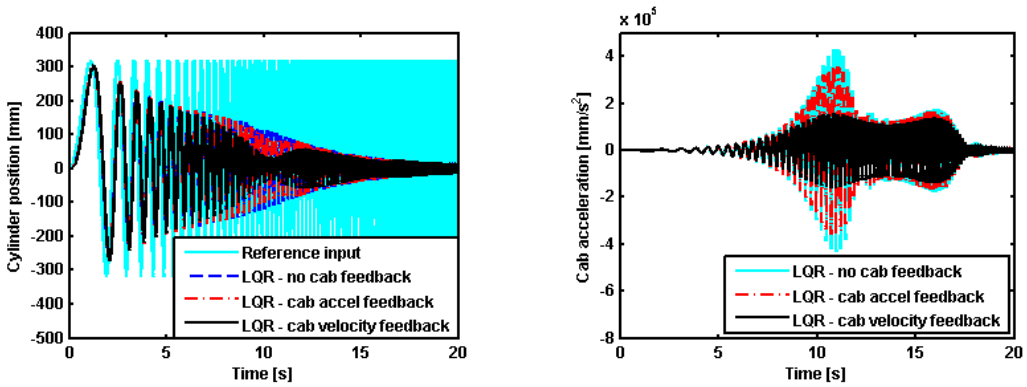

(a) Cylinder position

(b) Cab acceleration

Figure 32: Simulated response to swept sine input - LQR full state feedback controllers

terms for the measurements. These weightings were determined based on hardware experiments, in which measurement noise plays a significant role. The accelerometer signal is inherently very noisy in the case of acceleration measurement feedback, in spite of filtering. This noise produces shaky cylinder response in the hardware; therefore, in the acceleration feedback case, the weight for the cab vibration reduction was chosen to be lower than in the case of the smoother cab velocity feedback. In the subsequent human subject tests, only the cab velocity feedback was used.

In the case of the swept sine input, at some instants, the resulting cab acceleration signals include large signal power in the frequency range where the notch filter and input shaper can significantly diminish the output; this contributes to much more reduction in cab vibration with this input. In the case of the trapezoidal excitation, the cab acceleration signals include less signal power in the frequency range that is most heavily affected by the cab vibration compensators.

The next sections describe similar experiments performed on the hardware system. A more quantitative performance comparison is provided for the hardware testing.

5.4 PID Controller Hardware Testing

This section describes results from hardware testing for cylinder tracking performance and cab vibration compensation. A similar set of experiments was performed in hardware, including two cylinder position reference signals: a slowly varying smoothed-trapezoidal input and a swept sine input with a frequency range of 0.01 Hz to 8 Hz. For each controller and input combination, data were collected for a set of five runs at 30 seconds each.

Figure 33 shows the cylinder position tracking performance of the three PID-based controllers. As in the simulation, the system tracks this slowly varying signal well. There is a very small DC offset at each stop; this likely results from the valve deadband. The error signal reaches a point where it is small enough to produce a valve signal that remains within the deadband, and the small integration term in the PID controller is not sufficient to completely eliminate this effect.

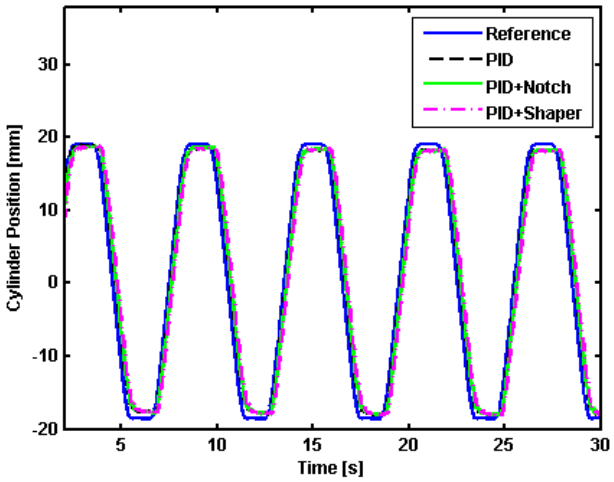

Figure 33: Hardware testing of PID controllers - cylinder position tracking of trapezoidal input

Figure 34 shows measured cab accelerations for the three controllers resulting from a trapezoidal cylinder input and a swept sine cylinder position input. All three controllers generally perform well in terms of cylinder position tracking, at least at a

very low frequency, and both the notch filter and input shaper are able to reduce cab vibration.

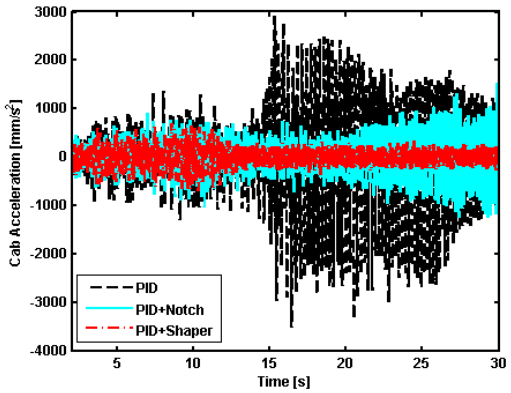

(a) Swept sine input

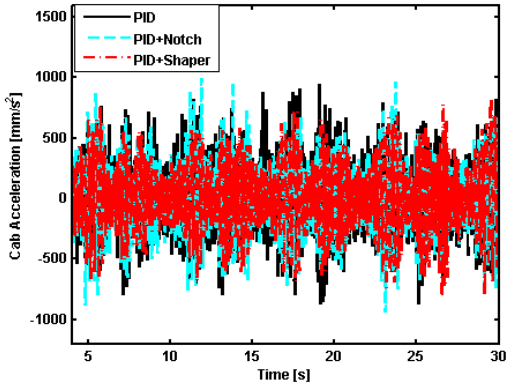

(b) Trapezoidal input

Figure 34: Hardware testing of PID controllers - cab accelerations for (a) swept sine input and (b) trapezoidal input

Tables 3 and 4 show the resulting mean squared errors in cylinder position tracking and cab acceleration, for each tested controller and input type. According to this test, in the case of the swept sine input, the input shaper produces the largest reduction in cab vibration as compared with the uncompensated PID controller, at 96%, and the notch filter produces a reduction of 83%. However, these reductions do come with a penalty in terms of speed of response. With the trapezoidal input, the tests do not show any decrease in cab vibration, but the differences in mean squared cab vibration are all less than 20%. The notch filter and input shaper compensators produce some

Table 3: Cylinder Tracking Mean Squared Errors - Classical Compensators (mm^2)

Controller	Trapezoidal Input	Swept Sine Input
PID	4.84	4.57
PID+Notch	7.72	2.75
PID+Shaper	14.63	2.62

Table 4: Mean Squared Cab Acceleration - Classical Compensators $((mm/s^2)^2)$ $(x10^5)$

Controller	Trapezoidal Input	Swept Sine Input
PID	0.65	6.98
PID+Notch	0.56	1.17
PID+Shaper	0.52	0.23

increase in mean squared tracking errors in the case of the trapezoidal input, and they produce a decrease in tracking errors with the swept sine input. Note that the errors are not normalized with respect to the amplitude of the input signal; while the data show larger tracking errors with the trapezoidal input, these are much smaller proportional to the reference signal amplitude.

5.5 Active Compensation Hardware Testing

The same set of experiments was performed on the hardware using the LQR state feedback controllers. Figure 35 shows the tracking response to a trapezoidal input for each compensator. As for the other controllers and the simulation, tracking performance is very similar for a slowly varying signal.

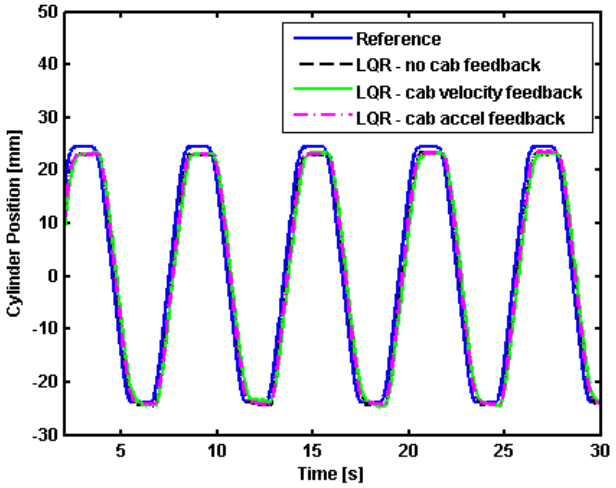

Figure 35: Hardware testing of LQR controllers - cylinder position tracking of trapezoidal input

Figure 36 shows the induced cab accelerations resulting from the swept sine and trapezoidal cylinder inputs. As in the case of the PID controllers, there is little difference between the induced cab vibrations for the case of the trapezoidal input. The LQR controllers do decrease the cab vibration with the sinusoidal input; however, they cause increased cab vibration at higher frequencies.

In the case of the swept sine input, Figure 36 shows a significant reduction cab vibration; however, as in simulation, the slow trapezoidal cylinder input shows little difference in cab vibration. In the case of the trapezoidal input, the cab vibrations are so small that the signal-to-noise ratio in the cab acceleration signal is low; this also contributes to the lack of cab vibration reduction in the case of the trapezoidal input.

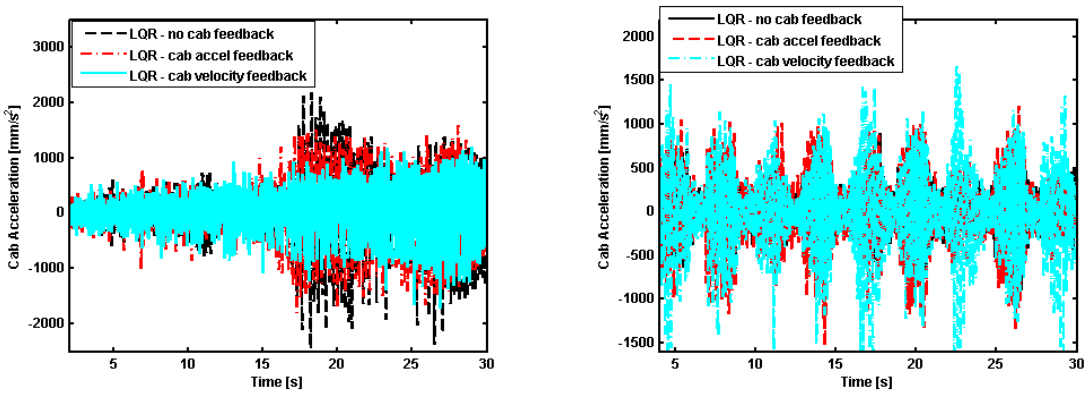

(a) Swept sine input

(b) Trapezoidal input

Figure 36: Hardware testing of LQR controllers - cab accelerations for (a) swept sine input and (b) trapezoidal input

Table 5: Cylinder Tracking Mean Squared Errors - State Space (mm^2)

Controller	Trapezoidal Input	Swept Sine Input
LQR - no cab feedback	15.26	3.08
LQR - cab velocity feedback	26.24	3.20
LQR - cab acceleration feedback	16.15	3.12

With the swept sine input, the LQR controller with cab velocity feedback produces a 49% reduction in cab vibration. As with the PID-based compensators, the compensators do degrade the cylinder tracking performance, but as shown in Figure 35, all three forms of the LQR controllers are able to track the trapezoidal input. In general, variations in mean squared cylinder position errors are small between the three types of LQR controllers. The cab vibration compensators do create slightly increased cab vibration in the case of the trapezoidal inputs; these likely result primarily from nonlinear effects. The next chapter describes the performance of these controllers in human-in-the-loop tracking experiments.

Table 6: Mean Squared Cab Acceleration - Active Compensators ($(mm/s^2)^2$) ($x10^5$)

Controller	Trapezoidal Input	Swept Sine Input
LQR - no cab feedback	0.48	2.52
LQR - cab velocity feedback	2.24	1.42
LQR - cab acceleration feedback	1.19	2.55

CHAPTER VI

HUMAN-IN-THE-LOOP EXPERIMENTS

6.1 Human-in-the-Loop Experiment

This chapter describes a set of human-in-the-loop experiments designed to test the performance of several controller-based methods for biodynamic feedthrough compensation. At this stage in the study on biodynamic feedthrough compensation, these compensators are developed only for a single degree-of-freedom, as described in Fig. 5. The operator controls only the boom cylinder within a range of approximately vertical to 40 degrees forward from vertical. Fore-aft motion of the input device commands motion of the boom cylinder.

The goal is to determine whether or not the controllers are able to improve the operator's ability to control the machine while seated on the tractor. In order to gauge the operator's ability to control the machine motion, it is necessary for the analysis to know exactly how the operator wants the machine to move. A number of types of human operator tests were possible. While it is desirable for the tests to mimic real operation as closely as possible, it is also desirable for the purpose of efficiency in the experiments that the tests create conditions under which biodynamic feedthrough is a problem. It is also necessary that learning effects are minimized as much as possible, and that the experiment provides a simple quantitative measure of operator performance. Three main types of tests were considered: (1) motion between desired waypoints, (2) tracking of a continuous time signal, and (3) tracking of a series of random magnitude steps under time constraints. The clearest method for giving the operator a distinctly specified task is to provide a tracking signal. But operation of backhoes tends to consist of motions between waypoints. Therefore, the

third test type was selected, tracking of a set of random magnitude steps.

This experiment is set up as a tracking-pursuit problem. The same set of experiments is performed at two operator stations, one on the tractor (with biodynamic feedthrough) and one beside the tractor at a desk (without biodynamic feedthrough). The two operator stations each have the same input device and a monitor displaying two signals, (1) the software generated tracking signal, and (2) the measured cylinder position, in real time.

The experiment tests five different controllers, all with position-position mapping between the input device and cylinder motion, (1) a PID cylinder position controller, (2) the same PID controller with a notch filter added near the structure natural frequencies, (3) the same PID controller with a ZV input shaper, (4) an LQR full state feedback cylinder position controller, and (5) the same LQR full state feedback controller with active vibration compensation added in the form of cab velocity feedback. Each test subject performs a test with each controller both on and off the tractor, totaling ten different tests.

The software generated tracking signal is comprised of a series of steps, each occurring at 2 second intervals, with random magnitudes. These commanded magnitudes are limited such that they remain within the desired range of motion of the machine. Each test lasts 140 seconds and tests a single controller type. Eight subjects were tested, although two subjects did not complete one of the ten tests. Subjects were not professional excavator operators, though some do have some experience using this machine interface.

Several measures were taken in order to minimize any learning effects. Each subject started with a practice session of approximately 2 minutes. During the experiments, the reference signal is generated randomly for every operator and every test. The signals are generated such that they have near zero mean and similar standard deviations, such that no controller receives more or less aggressive tracking signals.

Also, the controllers are presented to the operators in randomized order. Alternating test subjects started with the set of experiments on or off the tractor.

Figure 37: Operator station on tractor with monitor

Figure 37 shows the backhoe testbed with the monitor mounted in front of the operator's seat. The experiment includes the set of ten controller tests, plus a set of survey questions that the subjects fill out after each controller. The controllers are presented in random order, and the subjects are not aware of which controller is being tested. The full experiment takes approximately one hour per subject.

6.2 Experiment Results

This section describes the results from the tracking-pursuit experiments, in terms of cylinder tracking performance and cab acceleration excitation, the two outputs of the state space system. The results are measured in terms of two metrics: (1) mean squared cylinder position error, and (2) mean squared cab acceleration, measured over the entire test for each operator. These two metrics are computed for each operator with each controller, totaling 80 tests (minus two incomplete tests), or 78 data points for each metric.

Some results are given in the form of box-whisker plots. In these plots, the red line

in the center shows the median, the box indicates the 25th-to-75th percentile range, and outliers are denoted by x-marks. In the plots showing mean squared errors, smaller is better.

It should be noted that two forms of controllers are tested, a classical PID, with and without vibration compensation, and a full state feedback LQR controller, with and without vibration compensation. Each of these controller types allows for some tuning by the designer. The two types are not tuned to be equivalent in terms of speed of response; the LQR controller generally is tuned to be considerably faster and have higher gains. The PID controller was tuned on the hardware, which has some nonlinear effects and unmodeled dynamics, and these were found to result in some chatter and jittery response with PID control; in order to obtain smoother response, the PID controller was tuned to be slow. The LQR controller was roughly tuned in simulation with higher gains and then tuned more finely in the hardware using a coarse pattern search optimization. With the higher gains appeared to exhibit somewhat smoother response than a PID controller with the same bandwidth. It would be preferable for this study for the two types of controllers to have more similar speed of response.

In the following set of data on mean squared errors in cylinder tracking and cab acceleration, the key comparisons are between controllers of the same form with vibration compensated controllers and without vibration compensation, with the operator on the tractor. Note in particular the comparisons between the PID controller and PID with input shaper, and between the LQR controller with and without cab vibration feedback.

Figure 38 shows the mean squared cylinder position tracking error for each controller with the operator on the tractor. In general, in a system with flexibility, a slower or lower-gain controller which provides damping will perform better. In this

case, with the flexibility in the biodynamic feedthrough, the slower-tuned PID controller performs better. This does not necessarily generalize to a comparison between PID and full state feedback controllers, and it is separate from the comparison between the different forms of vibration compensation. In the PID case, the data show that the input shaper does slightly improve the operator's ability to track the reference, as compared with the PID without vibration compensation. In the LQR case, the active vibration compensation also provides improvement over LQR control without active damping. However, the sample size includes only eight participants, and the variations are large.

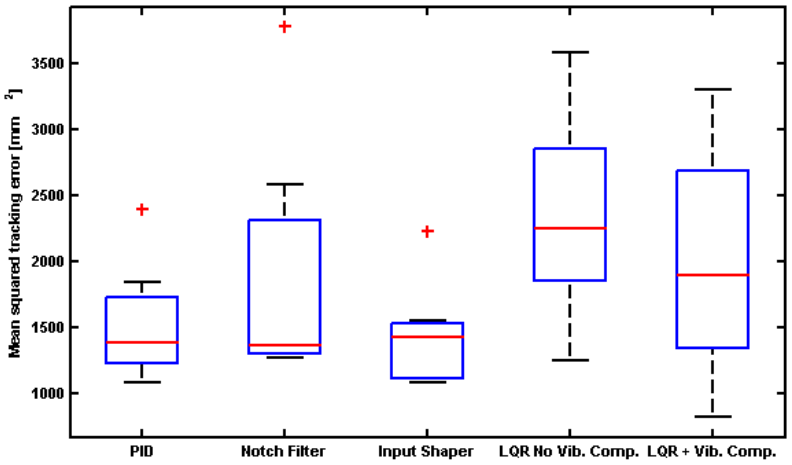

Figure 38: Human experiment mean squared cylinder tracking errors with operator seated on tractor

Figure 39 shows the mean squared cylinder tracking errors with the operator off the tractor. In general, this data illustrates the problem of biodynamic feedthrough; it shows that the operator performs better off the tractor with every controller. In this case, without the flexibility from the bioydnamic feedthrough, the faster LQR controller performs better.

Figure 40 shows the mean squared cab accelerations for each controller, with the operator on the tractor. These data also show that the input shaper provides some

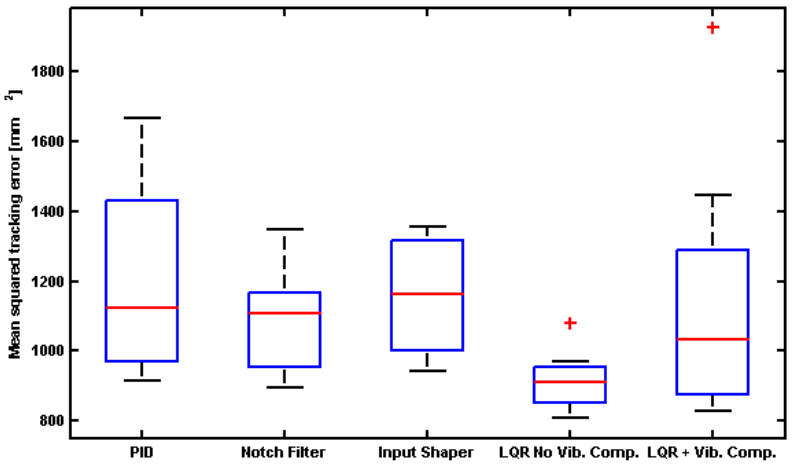

Figure 39: Human experiment mean squared cylinder tracking errors with operator seated off tractor

improvement over the basic PID controller, and the active vibration compensation provides some reduction in cab vibration as compared with the LQR without vibration compensation. Again, the faster LQR controllers excite more vibration. The active vibration compensation shows the largest variation in vibration reduction performance.

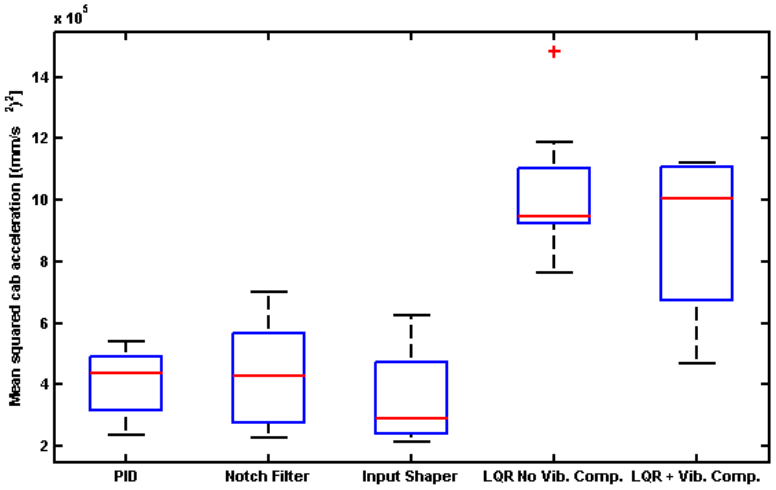

Figure 40: Human experiment mean squared cab accelerations with operator seated on tractor

Figure 41 shows the mean squared cab accelerations with the operator stationed off

the tractor. In this case, the variations within controller types are smaller, although there are outliers. The data indicate that all three types of vibration compensation do provide at least a slight reduction in mean squared cab acceleration.

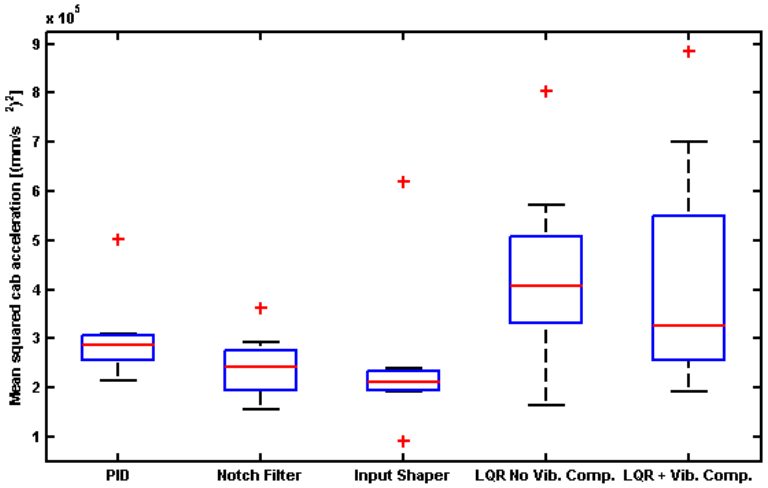

Figure 41: Human experiment mean squared cab accelerations with operator seated off tractor

These plots show significant variability and several outliers. While the individual outliers cannot be associated with any specific anomalies in testing, the outliers can generally be associated with several possible causes. First, operator performance did tend to improve over time; learning did occur over the course of the experiment. The order of presentation of the controllers was randomized such that this effect would be minimized in results data. However, some outliers may result from an operator's first or second test. Also, there were some large variations in time between experiments, allowing some operators to rest longer than others. Fatigue may have played a role with some operators.

Table 7 and Table 8 summarize the results from the previous plots. They show averages of the mean squared errors over the set of 8 subjects. In general, the data indicate that the input shaper and active vibration compensation approaches do provide some improvements in both cylinder tracking and cab vibration. The data also

Table 7: Cylinder Tracking Mean Squared Errors $[(mm^2)]$

Controller	Operator On Tractor	Operator Off Tractor
PID	152.6	120.4
PID + Notch Filter	188.3	108.6
PID + Input Shaper	143.9	115.7
LQR - No Cab Feedback	234.8	91.6
LQR + Cab Velocity Feedback	200.1	114.4

Table 8: Mean Squared Cab Acceleration $[(mm/s^2)^2]$ $(x10^5)$

Controller	Operator On Tractor	Operator Off Tractor
PID	4.08	3.02
PID + Notch Filter	4.35	2.43
PID + Input Shaper	3.55	2.48
LQR - No Cab Feedback	10.25	4.32
LQR + Cab Velocity Feedback	8.96	4.18

illustrate the problem resulting from biodynamic feedthrough. It should be noted that the biodynamic feedthrough gain K_{BF}, which refers to the mapping of the input device workspace to the machine workspace, is a parameter that can be adjusted by the designer. In this test setup, the nominal value of K_{BF} corresponds to the full size of the Omni workspace mapping to the full cylinder workspace. In order to ensure that the biodynamic feedthrough problem was significant, this gain was increased by approximately 30% in these experiments. This adjustment, in combination with the selected backhoe arm configuration, produce larger excitations of the cab that would be expected in normal operation. A larger sample size would be needed in order to determine statistical significance of the improvements resulting from the compensators.

6.3 Survey Results

After each controller test, the subjects were requested to fill out a survey. It asked for a rating of each controller, on and off the tractor, in terms of (1) accuracy, (2) speed of response, (3) smoothness, and (4) overall controllability, and it asked one

open-ended question about any likes/dislikes about that controller. The tracking-pursuit experiment provides a means to evaluate the operators' performance with each controller, while the survey provides information about their perception of their performance with each controller; often these serve different purposes.

Following is a series of box plots showing the operators' ratings of each controller, according to four different metrics. Note that in contrast to the previous series of box plots, in these cases, higher numbers are better. Figure 42 and Fig. 43 provide operator assessments of the accuracy provided by each controller, with the operator on and off the tractor, respectively. In general, while on the tractor, they rated all of the controllers similarly for this metric. Off the tractor, they rated the faster LQR controllers as more accurate.

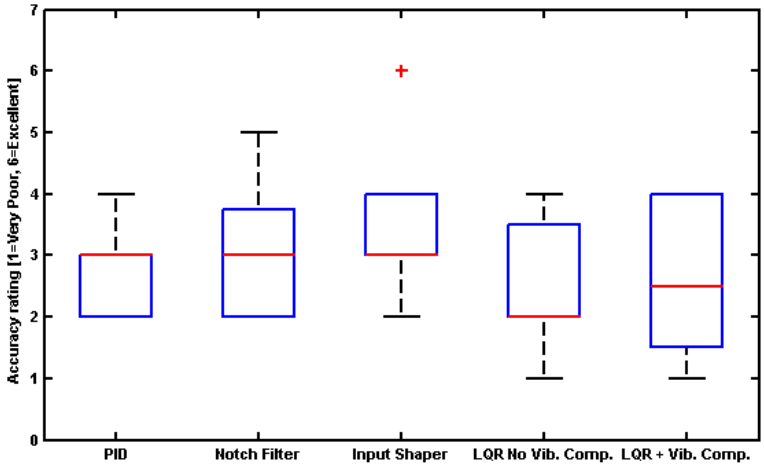

Figure 42: Survey results for operator on tractor: Accuracy

Similarly, Fig. 44 and Fig. 45 provide the operators' ratings of the controllers in terms of speed of response. The data show that they perceived the notch filter to be slower than other controllers. One interesting result here, in the case of the active vibration compensation, is that the operators perceived the vibration-compensated controller to be faster than the uncompensated LQR controller when they were on the tractor, and they perceived it to be relatively slower when they were off the tractor.

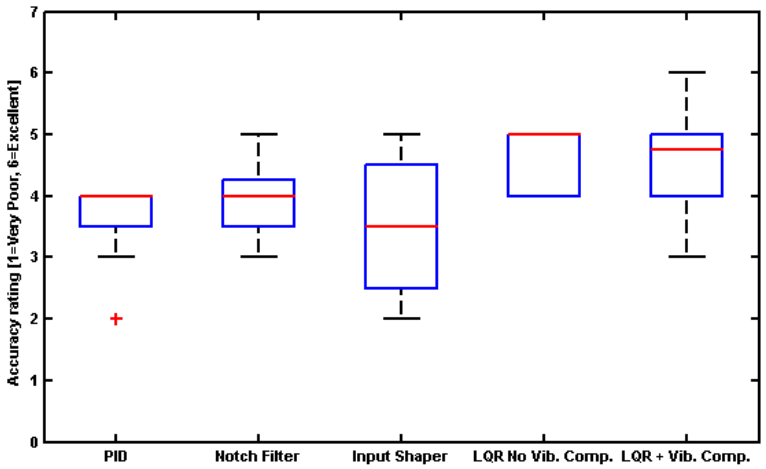

Figure 43: Survey results for operator off tractor: Accuracy

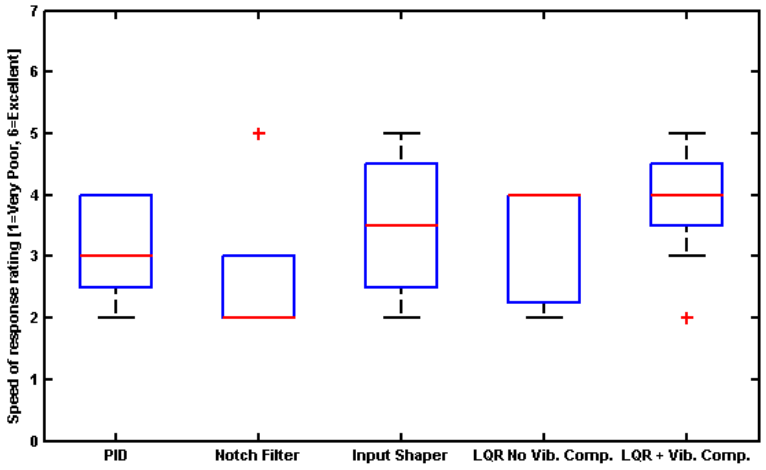

Figure 44: Survey results for operator on tractor: Speed of Response

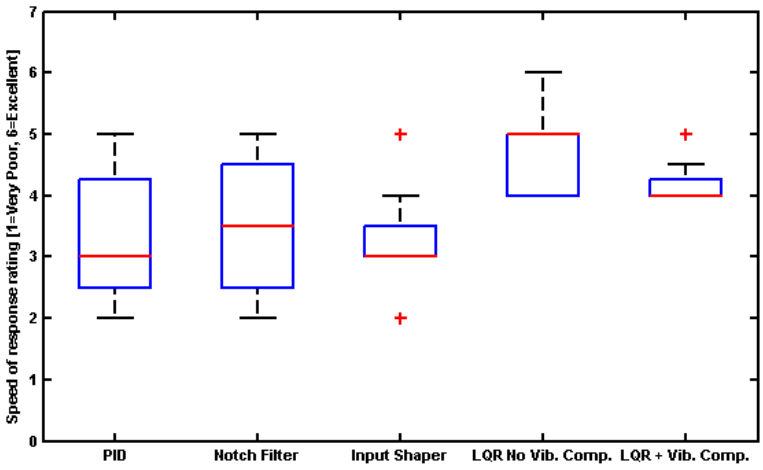

Figure 45: Survey results for operator off tractor: Speed of Response

Figure 46 and Fig. 47 show the operator ratings for smoothness, on and off the tractor. Off the tractor, they rate the five controllers similarly. However, when they are on the tractor, they rate the vibration compensated controllers as smoother than those without vibration compensation.

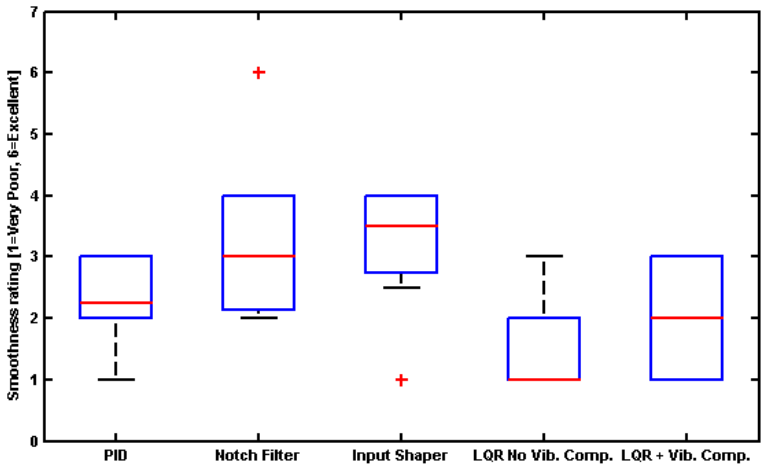

Figure 46: Survey results for operator on tractor: Smoothness

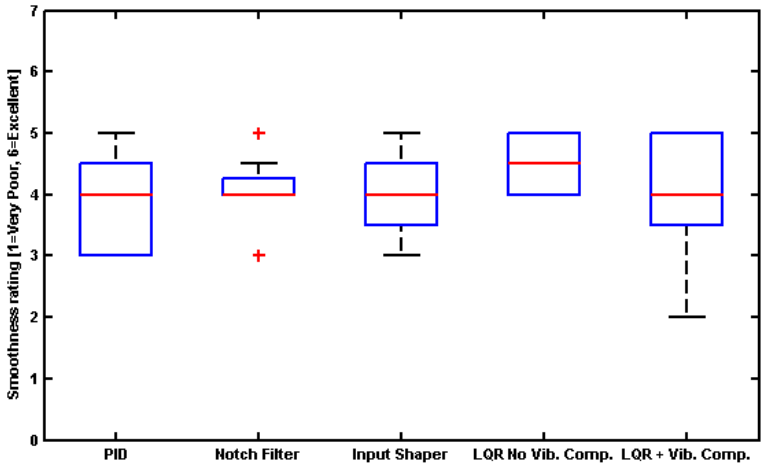

Figure 47: Survey results for operator off tractor: Smoothness

Figure 48 and Fig. 49 show the results for the final survey metric, overall controllability. In general, the operators do rate the controllers with vibration compensation at least slightly higher than those without compensation when they are on the tractor.

They rate the faster LQR controllers lower than the slower PID controllers when they are on the tractor, and they rate the LQRs higher off the tractor. On the tractor, they do rate input shaper and LQR compensators slightly higher than their counterparts without vibration compensation.

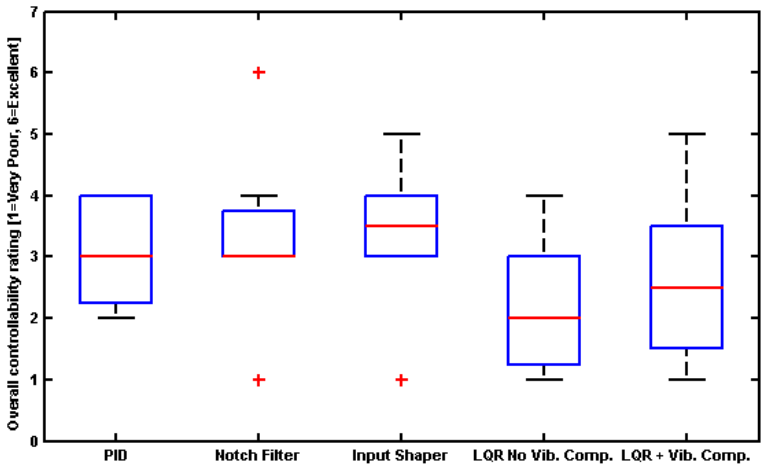

Figure 48: Survey results for operator on tractor: Overall Controllability

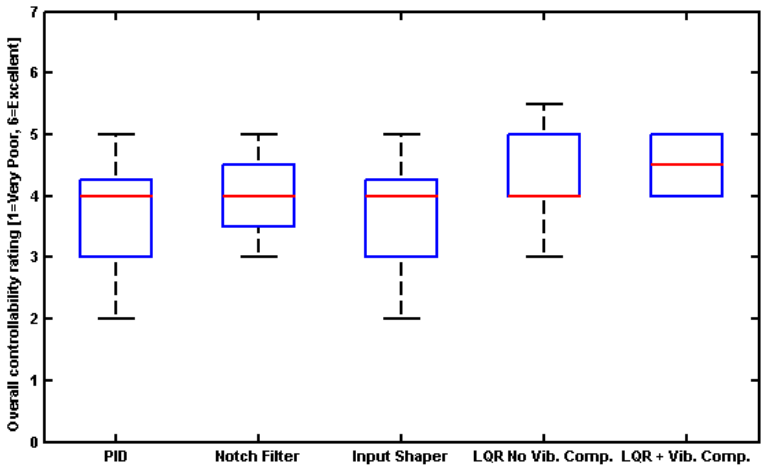

Figure 49: Survey results for operator off tractor: Overall Controllability

The next section describes some of the operators' comments to the open-ended questions about each controller.

6.3.1 Comments from open-ended questions

Operators provided a number of useful comments to the open ended questions about each controller.

- A few operators commented that they experienced large vibrations. Comments included, "I had to brace myself against the tractor" and that it "shook me out of my seat".

- With regard to the integrator effect of the PID controllers, with and without vibration compensation, operators noted that "it is hard to make small adjustments", that it is "too slow", and that "velocity saturates".

Operators could generally distinguish between the "slow" PID controllers and the "fast" LQR controllers, but they often commented that different versions of those controllers felt the same. They were not aware of what type of controller was being used during each test.

Based on these preliminary human subject experiments, some changes are suggested for future experiments. First, when designing PID controllers for manual control systems, it is not sufficient to tune the controllers manually to provide the best tracking performance to a software generated input; such resulting controllers may be ill-matched with the human operators' capabilities. In this case, the system with the PID controller acts as an integrator and is subsequently difficult for the human operator. This tuning can be adjusted. Second, the increase in the biodynamic feedthrough gain K_{BF} may have been too much; in these experiments, only very small hand motions are required to produce motion of the backhoe arm.

The next chapter discusses some conclusions, lessons learned and future work.

CHAPTER VII

CONCLUSIONS AND FUTURE WORK

7.1 Conclusions

This research provides several contributions; main areas are listed here.

- A dynamic model of a backhoe control system was developed and validated, including biodynamic feedthrough. Simulations based on these models produce results that match fairly well with the experimental results. Stability analysis was performed on the full models with biodynamic feedthrough. This system model is divided into a set of lumped parameter models of component dynamic systems, and it provides means for testing of a variety of compensation methods in simulation.

- Several different forms of controllers were evaluated both in simulations and in hardware. Results show that it is possible to develop controllers which move the backhoe arm such that cab vibration is significantly reduced. They also show that these reductions in cab vibration come at a cost in terms of cylinder position response. This reduction in cab vibration is beneficial both in terms of biodynamic feedthrough and ergonomics.

- Active vibration compensation using cab acceleration feedback was implemented in the backhoe system, and results show that the active vibration compensation approach can significantly reduce cab vibration. The active vibration compensation approach is based on the system model.

- A small set of human subject tests were performed. They show clearly that biodynamic feedthrough does degrade the operator's ability to control the machine

while seated on the tractor. They also indicate that the input shaper and active vibration compensation approaches do provide some improvement in both cab vibration and the operator's cylinder tracking ability.

This work provides a preliminary study on a very complex problem. There are a number of open questions remaining. Further development is required before a biodynamic feedthrough compensating controller could be applied to a working construction machine.

7.2 Future Work

A number of areas for further research are needed before these compensation methods could be successfully implemented on backhoes in industry.

- Steps must be taken to expand the biodynamic feedthrough compensation to work in all six degrees of freedom, in all possible backhoe arm configurations throughout the machine workspace. The valve/cylinder and structure dynamics vary depending on the configuration of the backhoe arm. This may be achievable using adaptation based on system measurements. An adaptive input shaper, adaptive filter, or adaptive active damping approach could be implemented. Some preliminary experiments indicate that decoupling the degrees of freedom is not a good approximation. For instance, fore-aft motion of the backhoe arm creates a rocking motion in the human body, which includes both fore-aft and vertical components. Interactions between degrees of freedom should be considered.

- Many of the parameters in this system are expected to vary widely. Extensive analysis of robustness to such variations is critical. For instance, human body parameters vary from person to person, with fatigue, and with activity level, among others. The backhoe system dynamics can vary depending on the loading

conditions, use of outriggers, soil conditions, etc. The system models with biodynamic feedthrough tend to be near the verge of instability; these analyses are needed in order to ensure stability.

- It may be possible to achieve improved results with active compensation, particularly cab acceleration feedback, if a Kalman Filter observer was implemented.

- In order to determine the balance between cab vibration reduction and cylinder position tracking performance, it would be helpful to understand what are the necessary control performance criteria for a manually controlled backhoe system, particularly in terms of bandwidth. It would be helpful to know how much reduction in speed of response is acceptable to human operators.

- These models assume that the human is a purely mechanical system. Human cognition is used only to generate a reference signal; no cognitive or neuromuscular feedback is considered. According to [14], this is a reasonable assumption in biodynamic feedthrough since the unwanted hand motions tend to occur primarily at frequencies higher than the cognitive bandwidth; in other words, the frequency content of the signals in the biodynamic feedthrough are faster than the human's ability to compensate. However, the human cognitive and neuromuscular feedback signals do affect the overall system dynamics, and they should be considered in the design of the controllers.

Biodynamic feedthrough creates a problem in industry standard velocity controlled systems using joysticks. It is a more significant problem and a major barrier for the new, more intuitive coordinated position controllers. This research presents a first step toward mitigating the problem of biodynamic feedthrough in backhoe operation and a step toward overcoming this barrier for implementation of advanced user interfaces such as the Haptically Enhanced Robotic Excavator (HEnRE) system.

APPENDIX A

MATLAB CODE FOR SYSTEM MODEL, CONTROLLER AND OBSERVER CALCULATIONS

```
%%%%%%%%%%%%%%%%%%%%%%%%%%%%%%%%%%%%%%%%%%%%%%%%%%%%%%%%%%%%%%%%%%%%%%%
% MATLAB file to compute LQR gains and observer parameters
% By: Heather Humphreys
% Last edited: Oct. 22, 2010
%%%%%%%%%%%%%%%%%%%%%%%%%%%%%%%%%%%%%%%%%%%%%%%%%%%%%%%%%%%%%%%%%%%%%%%


clc;
close all;
%clear all;


load('D:\HF_HEnRE_hch\BoomControl\Modeling\ModelData_Boom_...
062210_TFData_Upd081410.mat');
load('D:\HF_HEnRE_hch\BoomControl\Control\Trapez4.mat');


%%%%%%%%%%%%%%%%%%%%%%%%%%%%%%%%%%%%%%%%%%%%%%%%%%%%%%%%%%%%%%%%%%%%%%%
% Inner cab velocity feedback loop
%%%%%%%%%%%%%%%%%%%%%%%%%%%%%%%%%%%%%%%%%%%%%%%%%%%%%%%%%%%%%%%%%%%%%%%


VCBoomnum_vel = VCBoomnum(2:4);
VCBoomden_vel = VCBoomden(1:3);
```

```
tfvc_vel = tf(VCBoomnum_vel,VCBoomden_vel);

Kp_var = .25;
Kp = Kp_var/(VCBoomnum_vel(3)/VCBoomden_vel(3));

CLTF_Kp_VC = feedback(tfvc_vel*Kp,1);
[CLTF_Kp_VC_num, CLTF_Kp_VC_den] = tfdata(CLTF_Kp_VC,'v')

k_sserr = 1;

%%%%%%%%%%%%%%%%%%%%%%%%%%%%%%%%%%%%%%%%%%%%%%%%%%%%%


%%%%%%%%%%%%%%%%%%%%%%%%%%%%%%%%%%%%%%%%%%%%%%%%%%%%%%%%%%
% 7-state valve/cylinder and structure model
% with inner feedback loop
% outputs: cab velocity and cylinder position
%%%%%%%%%%%%%%%%%%%%%%%%%%%%%%%%%%%%%%%%%%%%%%%%%%%%%%%%%%
APlant = [[0,1,0,0,0,0,0];...
    [0,0,1,0,0,0,0];...
    [0,0,0,1,0,0,0];...
    [-wns1^2 *wns2^2,-2 *zetas1 *wns1 *wns2^2-2 *wns1^2 *zetas2...
     *wns2,-wns2^2-4 *zetas1 *wns1 *zetas2 *wns2-wns1^2,-2 *zetas2...
     *wns2-2 *zetas1 *wns1,Ks *wns1^2 *wns2^2,2 *Ks *zetas1 *wns1...
     *wns2^2+2 *Ks *wns1^2 *zetas2 *wns2,4 *Ks *zetas1 *wns1...
     *zetas2 *wns2];...
    [0,0,0,0,0,1,0];...
```

```
    [0,0,0,0,0,0,1];...
    [0,0,0,0,0,-wnvc^2,-2 *zetavc *wnvc]];
BPlant = [[0];[0];[0];[0];[0];[0];[Kvc*wnvc^2]];

A1 = [[0,1,0,0,0,0,0];...
    [0,0,1,0,0,0,0];...
    [0,0,0,1,0,0,0];...
    [-wns1^2 *wns2^2,-2 *zetas1 *wns1 *wns2^2-2 *wns1^2 *zetas2...
     *wns2,-wns2^2-4 *zetas1 *wns1 *zetas2 *wns2-wns1^2,-2 *zetas2...
     *wns2-2 *zetas1 *wns1,Ks *wns1^2 *wns2^2,2 *Ks *zetas1 *wns1...
     *wns2^2+2 *Ks *wns1^2 *zetas2 *wns2,4 *Ks *zetas1 *wns1...
     *zetas2 *wns2];...
    [0,0,0,0,0,1,0];...
    [0,0,0,0,0,0,1];...
    [0,0,0,0,0,-Kp*Kvc*wnvc^2-wnvc^2,-2 *zetavc *wnvc]];
B1 = [[0];[0];[0];[0];[0];[0];[Kp*Kvc*wnvc^2]];

C1 = [0,0,0,0,1,0,0];
D1 = 0;

C1sim = eye(7);
D1sim = [0;0;0;0;0;0;0];

C1MIMO = [0,0,0,0,1,0,0;...
0,1,0,0,0,0,0];
C1MIMOacc = [0,0,0,0,1,0,0;...
0,0,1,0,0,0,0];
```

```
D1MIMO = [0;0];

SysMIMO_ss = ss(A1,B1,C1MIMO,D1MIMO);

%States:
% x1 = structure position
% x2 = structure vel
% x3 = structure accel
% x4 = structure jerk
% x5 = cylinder pos
% x6 = cylinder vel
% x7 = cylinder accel
%%%%%%%%%%%%%%%%%%%%%%%%%%%%%%%%%%%%%%%%%%%%%%%%%%%%%%%


%%%%%%%%%%%%%%%%%%%%%%%%%%%%%%%%%%%%%%%%%%%%%%%%%%%%%%%%%%
% Check stability
%%%%%%%%%%%%%%%%%%%%%%%%%%%%%%%%%%%%%%%%%%%%%%%%%%%%%%%%%%
fprintf('eigs A: \n')
eigs(A1)
% stable.

fprintf('sys tf: \n')
[SysTFnum,SysTFden] = ss2tf(A1,B1,C1,D1)
SysTF = tf(SysTFnum,SysTFden)

%%%%%%%%%%%%%%%%%%%%%%%%%%%%%%%%%%%%%%%%%%%%%%%%%%%%%%%%%%%%%%%%
```

```
%Compute Nbar
%neglects cab vibration measurement - no reference cab vibration
%%%%%%%%%%%%%%%%%%%%%%%%%%%%%%%%%%%%%%%%%%%%%%%%%%%%%%%%%%%%%%%%%%%%%%%
N2 = ([A1,B1;C1MIMO(1,:),D1MIMO(1,:)]^(-1))*[0;0;0;0;0;0;0;1];
Nx = N2(1:7);
Nu = N2(8);



%%%%%%%%%%%%%%%%%%%%%%%%%%%%%%%%%%%%%%%%%%%%%%%%%%%%%%%%%%%%%%%%%%%%%%%
% Controllability and Observability
%%%%%%%%%%%%%%%%%%%%%%%%%%%%%%%%%%%%%%%%%%%%%%%%%%%%%%%%%%%%%%%%%%%%%%%
%Observability:
ObsMIMO = [C1MIMO;C1MIMO*A1;C1MIMO*A1*A1;C1MIMO*A1*A1*A1;C1MIMO*A1...
*A1*A1*A1;C1MIMO*A1*A1*A1*A1*A1;C1MIMO*A1*A1*A1*A1*A1*A1...
;C1MIMO*A1*A1*A1*A1*A1*A1*A1]
fprintf('MIMO Observability Rank: \n')
rank(ObsMIMO)
%Controllability:
Cont = [B1, A1*B1, A1*A1*B1, A1*A1*A1*B1, A1*A1*A1*A1*B1,...
A1*A1*A1*A1*A1*B1, A1*A1*A1*A1*A1*A1*B1, A1*A1*A1*A1*A1*...
A1*A1*B1]
fprintf('Controllability Rank: \n')
rank(Cont)
% Seems completely controllable


%%%%%%%%%%%%%%%%%%%%%%%%%%%%%%%%%%%%%%%%%%%%%%%%%%%%%%%%%%%%%%%%%%%%%%%
% Controller gains
```

```
%%%%%%%%%%%%%%%%%%%%%%%%%%%%%%%%%%%%%%%%%%%%%%%%%%%%%%%%%%%%%%%%%%%%%%%
%Get LQR Gains
Rlqr = 1;
%CScale = [40,0;0,0];
CScale = [40,0;0,2]; % 50 way upper limit
Qlqr = (CScale*C1MIMO)'*(CScale*C1MIMO) ;
Nlqr=0;
[K,S,e] = LQR(A1,B1,Qlqr,Rlqr,Nlqr)

ContStability = eigs(full(A1-B1*K))
KSysMIMO_ss = ss(A1-B1*K,B1,C1MIMO,0)
% still stable.



%%%%%%%%%%%%%%%%%%%%%%%%%%%%%%%%%%%%%%%%%%%%%%%%%%%%%%%%%%%%%%%%%%%%%%%
% Observer
%%%%%%%%%%%%%%%%%%%%%%%%%%%%%%%%%%%%%%%%%%%%%%%%%%%%%%%%%%%%%%%%%%%%%%%
C1ObsSim = eye(7);
C1Obs = C1MIMO;

%Assigned Observer Poles:
DesiredObsPoles = [-180,-190,-191,-175,-176,-195,-196]

[Lt,precL,messageL] = place(A1',C1Obs',DesiredObsPoles);

L = Lt';
fprintf('Obs Stability\n')
```

```
eigs(A1-L*C1Obs)
ObsStability = eigs(A1-B1*K-L*C1Obs)

A1Obs = [A1-L*C1Obs];
B1Obs = [B1, L];
D1Obs = [0];
D1ObsSim = [0,0,0;0,0,0;0,0,0;0,0,0;0,0,0;0,0,0;0,0,0;0,0,0;0,0,0]

LSysMIMO_ss = ss(A1Obs,B1Obs,C1Obs,D1Obs)

% CHECKS
[SysTFp,SysTFz]=pzmap(SysTF);



%%%%%%%%%%%%%%%%%%%%%%%%%%%%%%%%%%%%%%%%%%%%%%%%%%%%%%%%%%%%%%%%%%%%%%%
% Full system dynamics
%%%%%%%%%%%%%%%%%%%%%%%%%%%%%%%%%%%%%%%%%%%%%%%%%%%%%%%%%%%%%%%%%%%%%%%
% *from franklin & powell, p. 536
% *case 1 (fig. 2), M=-B*N
CFull = [0,1,0,0,0,0,0];
AFullSys = [(A1-B1*K),-B1*K;zeros(7),(A1-L*C1MIMO)]
BFullSys = [B1;B1]
CFullSys = [CFull,zeros(1,7)]
DFullSys = zeros(1,1);

FullSysMIMO = ss(AFullSys, BFullSys, CFullSys, DFullSys);
[FullSysMIMOTFnum,FullSysMIMOTFden] = ss2tf(AFullSys, BFullSys,
```

```
CFullSys, DFullSys)
FullSysMIMOTF = tf(FullSysMIMOTFnum,FullSysMIMOTFden);


eig(AFullSys)
figure, pzmap(FullSysMIMO)


%ADD HUMAN
Human = 0.56/(s^2);
Kbf = 0.6;
SyswHuman = feedback(Kbf*FullSysMIMOTF,Human);


%%%%%%%%%%%%%%%%%%%%%%%%%%%%%%%%%%%%%%%%%%%%%%%%%%%%%%%%%%%%%%%%%%%%%%%
% End
%%%%%%%%%%%%%%%%%%%%%%%%%%%%%%%%%%%%%%%%%%%%%%%%%%%%%%%%%%%%%%%%%%%%%%%
```

APPENDIX B

SIMULINK DIAGRAMS

Simulink Subsystem for LQR Controller with Cab Velocity Feedback

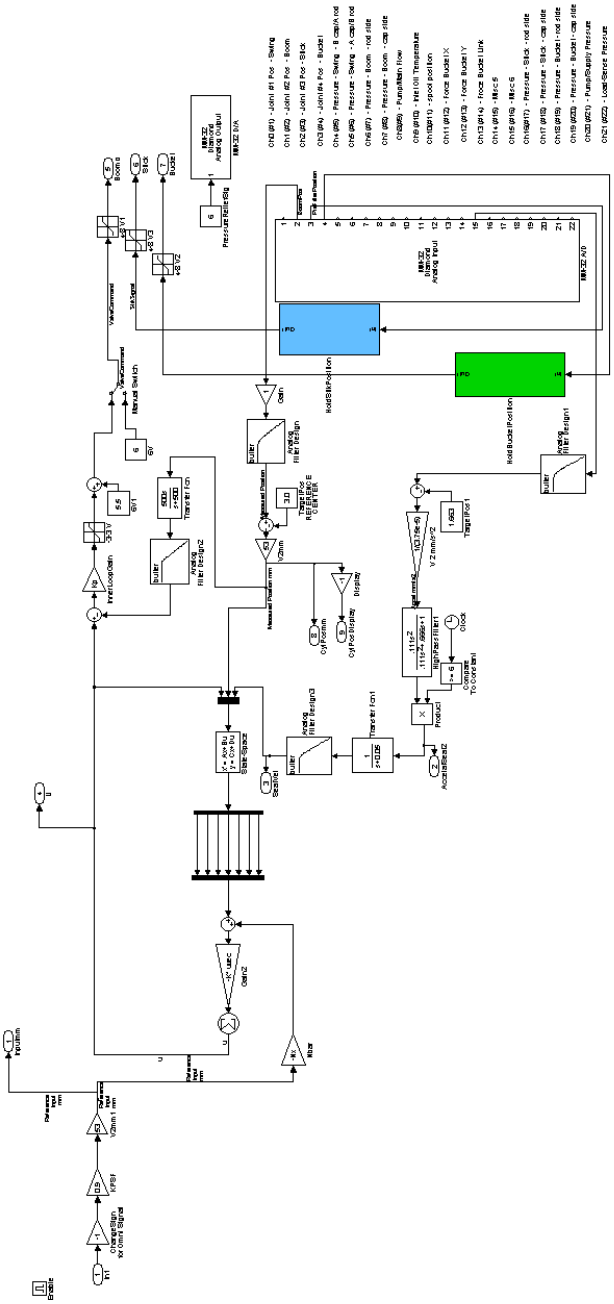

Simulink System for Control of Backhoe Arm with SensAble Omni Input

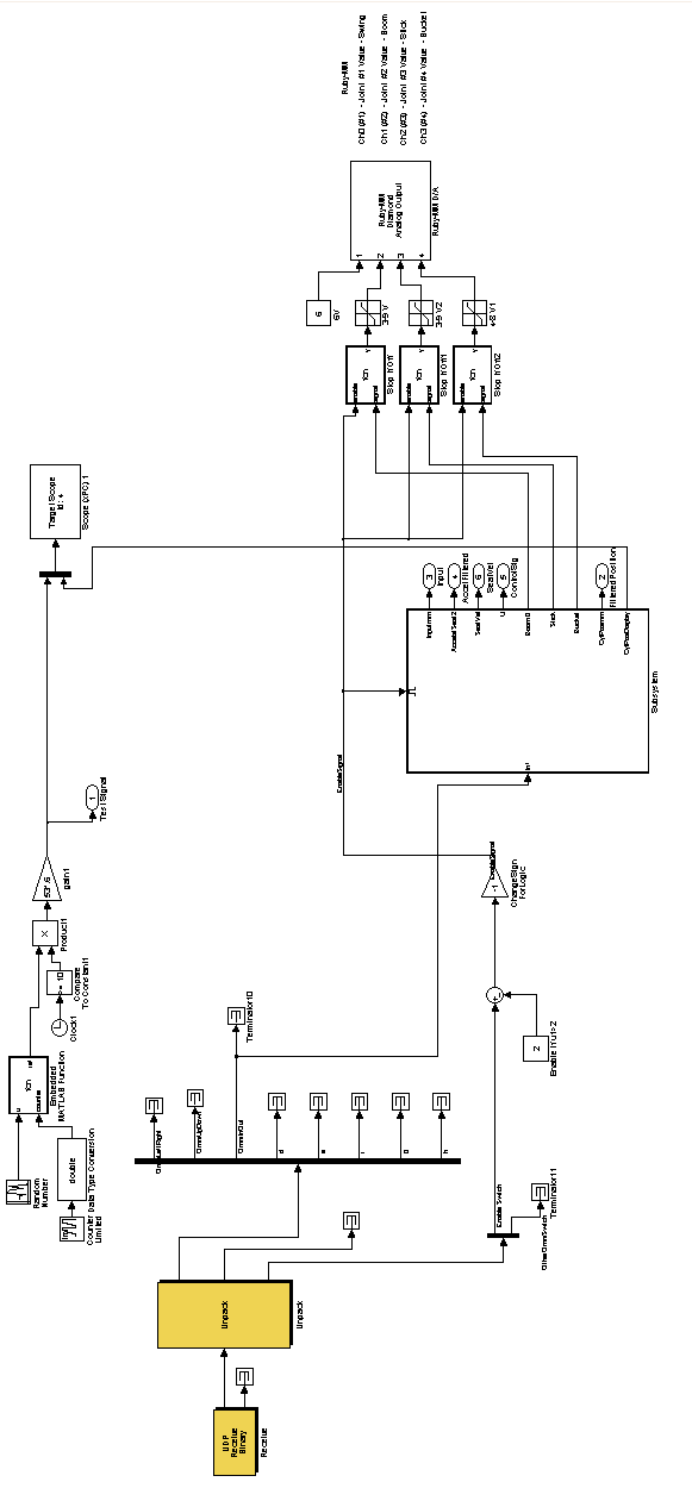

APPENDIX C

HUMAN SUBJECT TEST PROTOCOL

This step-by-step protocol was used for eight human subjects in a graphical user interface based single-cylinder tracking experiment, based on the IRB approval.

1. First, subjects were given a consent form which explains the test procedure and any potential risks.

2. An overview of the test was provided by the test administrator, including the functions of the input device, the tracking signals on the computer screen, and the backhoe arm itself.

3. Subjects ran the tracking experiment off the tractor for 2 minutes as a practice session, in order to become familiar with the setup.

4. The starting operating station on the tractor or off the tractor was alternated between test subjects, to minimize effects of learning. Each subject performed a set of five tracking experiments in the designated starting station. The controllers were presented in random order. They were asked to fill out a set of survey questions after each controller.

5. Subjects moved to a different operating station and ran the same experiment with the same five controllers, presented in a different random order. This completed the experiment.

REFERENCES

[1] Allen, R. W., Jex, H. R., and Magdaleno, R. E., "Manual control performance and dynamic response during sinusoidal vibration," Tech. Rep. AMRL-TR-73-78, STI-TR-1013-2, 1973.

[2] Anthonis, J. and Ramon, H., "Design of an active suspension to suppress the horizontal vibrations of a spray boom," *Journal of Sound and Vibration*, vol. 266, pp. 573–583, 2003. added hardware active suspension - like active vibration isolation, used H-inf.

[3] Arai, F., Tateishi, J., and Fukuda, T., "Dynamical analysis and suppression of human hunting in the excavator operation," in *IEEE Intl. Workshop on Robot and Human Interactive Communication*, (Osaka, Japan), pp. 394–399, 2000.

[4] Book, W. J., "Controlled motion in an elastic world," *ASME Journal of Dynamic Systems Measurement and Control*, 1993.

[5] Enes, A. and Book, W., "Blended shared control of zermelo's navigation problem," in *American Control Conference*, (Baltimore, MD), 2010.

[6] Enes, A. and Book, W., "Towards shared control of hydraulic excavators," in *Fluid Power Net International 6th Annual PhD Symposium*, (West Lafayette, IN), 2010.

[7] Enes, A., Elton, M., and Book, W., "A virtual reality operator interface station with hydraulic hardware-in-the-loop simulation for prototyping excavator control systems," in *IEEE Advanced Intelligent Mechatronics*, (Singapore), 2009.

[8] Frankel, J. G., *Development of a Haptic Backhoe Testbed*. PhD thesis, Georgia Tech, 2007.

[9] Franklin, C. and Powell, J., *Feedback Control of Dynamic Systems*. 1987.

[10] Gopala Rao, L. V. V. and Narayanan, S., "Sky-hook control of nonlinear quarter car model traversing rough road matching performance of lqr control," *Journal of Sound and Vibration*, vol. 323, pp. 515–529, 2009.

[11] Humphreys, H. C. and Book, W. J., "Possible methods for biodynamic feedthrough compensation in backhoe operation," in *Fluid Power Net International 6th Annual PhD Symposium*, (West Lafayette, IN), 2010.

[12] Humphreys, H. C., Book, W. J., and Huggins, J. D., "Modeling of biodynamic feedthrough in backhoe operation," in *ASME Dynamic Systems and Control Conference*, (Hollywood, CA), 2009.

[13] Humphreys, H. C., Book, W. J., and Huggins, J. D., "Compensation for biodynamic feedthrough in backhoe operation by cab vibration control," in *International Conference on Robotics and Automation*, (Shanghai), 2011.

[14] Jex, H. R. and Magdaleno, R. E., "Biomechanical models for vibration feedthrough to hands and head for a semisupine pilot," *Aviation, Space and Environmental Medicine*, vol. 49, no. 1, pp. 304–316, 1978.

[15] Kelps, I. and et. al., "Measurement of hybridiii dummy properties and analytical simulation data base development," Tech. Rep. AAMRL-TR-88-005, Armstrong Aerospace Medical Research Laboratory, Feb. 1988 1988.

[16] Kontz, M. E. and Book, W. J., "Haptic enhancement of hydraulic equipment," in *FPNI-PhD Symposium*, (Sarasota, FL), pp. 497–506, 2006.

[17] Kontz, M. E. and Book, W. J., "Electronic control of pump pressure for a small haptic backhoe," *Intl. Journal of Fluid Power*, vol. 8, 2007.

[18] Kontz, M. E. and Book, W. J., "Flow control for coordinated motion and haptic feedback," *Intl. Journal of Fluid Power*, vol. 8, no. 2, pp. 5–16, 2007.

[19] Kontz, M. E., Herrera, M. C., Huggins, J. D., and Book, W. J., "Impedance shaping for improved feel in hydraulic systems," in *ASME Intl. Mech. Engr. Congr. Expo.*, vol. FPST-Vol. 14, (Seattle, WA), 2007.

[20] Kontz, M. E., *Haptic Control of Hydraulic Machinery Using Proportional Valves*. PhD thesis, Georgia Tech, 2007.

[21] Lawrence, P. D. and et. al., "Coordinated and force-feedback control of hydraulic excavators," in *Fourth International Symposium on Experimental Robotics*, (Stanford, CA), 1995.

[22] LifeModeler, *LifeMOD User's Manual 2008*. 2008.

[23] Magee, D. P. and Book, W. J., "Optimal arbitrary time delay (oat) filter and method to minimize unwanted system dynamics," June 20, 2000 2000. U.S. Patent No. 6,078,844.

[24] Margolis, D. and Shim, T., "Instability due to interacting hydraulic and mechanical dynamics in backhoes," *Journal of Dynamic Systems and Control*, vol. 125, pp. 497–504, 2003.

[25] Rahmfeld, R. and Ivantysynova, M., "An overview about active oscillation damping of mobile machine structure," *Intl. Journal of Fluid Power*, vol. 5, no. 2, pp. 5–24, 2004.

[26] Repperger, D. W., "Biodynamic resistant control stick," 1984. U.S. Patent No. 4,477,043.

[27] Sheridan and Ferrell, *Man-Machine Systems*. 1974.

[28] Siciliano, B. and Khatib, O., *Springer Handbook of Robotics*. 2008.

[29] Singer, N. and Seering, W. P., "Preshaping command inputs to reduce system vibration," *ASME Journal of Dynamic Systems and Control*, 1990.

[30] Singhose, W. and Seering, W., *Command Generation for Dynamic Systems*. 2007.

[31] Sirouspour, M. R. and Salcudean, S. E., "Suppressing operator-induced oscillations in manual control systems with moveable bases," *IEEE Transactions on Control Systems Technology*, vol. 11, no. 4, pp. 448–459, 2003.

[32] Sovenyi, S. and Gillespie, R. B., "Cancellation of biodynamic feedthrough in vehicle control tasks," *IEEE Transactions on Control Systems Technology*, vol. 15, no. 6, pp. 1018–1029, 2007.

[33] Truckenbrot, A., "Modeling and control of flexible manipulator structures," in *4th CISM-IFToMM Ro. Man. Sy.*, (Zabrow), 1981.

[34] van Passen, M. M., van der Vaart, J. C., and Mulder, J. A., "Model of the neuromuscular dynamics of the human pilot's arm," *Journal of Aircraft*, vol. 41, no. 6, pp. 1482–1486, 2004.

[35] Williamson, C., Lee, S., and Ivantysynova, M., "Active vibration damping for an off-road vehicle with displacement controlled actuators," *Intl. Journal of Fluid Power*, vol. 10, no. 3, pp. 5–16, 2009.

[36] Williamson, C. A., *Active Vibration Damping for a Skid-Steer Loader Using Displacement-Controlled Actuators*. PhD thesis, Purdue University, 2007.

[37] Zatiorsky, V. M., *Kinetics of Human Motion*. Sheridan Books, 2002.